literature, showing that though VEGF, TGFβ-1, bFGF, and EGF positively correlated with hCG [17,61,62], TNFα expression is attenuated by hCG [63].

Our morphologic data, especially those from SEM of vcc, clearly confirmed that mRNAs of the studied angiogenic factors are hereafter translated to become functionally active, as demonstrated by the formation of the rich and angiogenically active microvascular network only in the T4-treated group. Similar to what was found in control rats in the ultrastructural study, activated capillaries, arterioles and venules—often accompanied by the presence of recruited pericytes and swollen smooth muscle cells, respectively—were frequently observed in the developing CL of group 3 rats. On the contrary, in gonadotropin-treated *rdw* rats (group 2) any developing CL was found and several atretic FLs were present in the ovaries. Quiescent endothelial cells, rarely surrounded by pericytes provided with short cytoplasmic extensions, were observed. From these results it is indeed clear that the presence of an adequate hormonal supply, as already demonstrated in other experimental models [33,64], supports the physiologic evolution of FL and CL development associated with an intensive angiogenesis that, with dynamic remodeling, sustains the fast evolution of the quiescent early periovulatory FL in a highly vascularized CL [65].

5. Conclusions

Morphologic, quantitative, and molecular data clearly indicated for the first time that T4 plays an important role in stimulating luteal angiogenesis in gonadotropin-primed hypothyroid *rdw* rats. The early CL development is associated with a T4-mediated induction of luteal angiogenesis involving pericyte activation and upregulation of major growth factors implicated in the regulation of angiogenesis, such as VEGF and bFGF. The molecular mechanisms involved in these morphologic differentiations need to be further investigated even if these data confirmed that the consolidation of a well developed vascular network is necessary for the early CL development [19,36].

Acknowledgments

The authors thank Dr. Jin-Yi Jiang for his precious contribution to this research, especially for the study design and molecular study, Dr. Tiziana Stallone for her technical contribution in the transmission electron microscopy study, and Prof. Maria Silvia Marottoli for her revision of the English language version of the manuscript.

Funds were provided by the Italian Ministry for University and Research: University of L'Aquila and University of Rome - La Sapienza; Italian National Council of Research (CNR); and the Japanese Society for Promotion of Sciences (JSPS).

References

[1] Macchiarelli G. The microvasculature of the ovary: a review by SEM of vascular corrosion casts. J Reprod Dev 2000;46:207–25.
[2] Plendl J. Angiogenesis and vascular regression in the ovary. Anat Histol Embryol 2000;29:257–66.
[3] Reynolds LP, Grazul-Bilska AT, Redmer DA. Angiogenesis in the female reproductive organs: pathological implications. Int J Exp Pathol 2002;83:151–63.
[4] Macchiarelli G, Jiang JY, Nottola SA, Sato E. Morphological patterns of angiogenesis in ovarian follicle capillary networks. A scanning electron microscopy study of corrosion cast. Microsc Res Tech 2006; 69:459–68.
[5] Macchiarelli G, Nottola SA, Palmerini MG, Bianchi S, Maione M, Lorenzo C, et al. Morphological expression of angiogenesis in the mammalian ovary as seen by SEM of corrosion casts. Ital J Anat Embryol 2010;115:109–14.
[6] Macchiarelli G, Nottola SA, Vizza E, Kikuta A, Murakami T, Motta PM. Ovarian microvasculature in normal and hCG stimulated rabbits. A study of vascular corrosion casts with particular regard to the interstitium. J Submicrosc Cytol Pathol 1991;23:391–5.
[7] Macchiarelli G, Nottola SA, Vizza E, Familiari G, Kikuta A, Murakami T, et al. Microvasculature of growing and atretic follicles in the rabbit ovary: a SEM study of corrosion casts. Arch Histol Cytol 1993;56:1–12.
[8] Macchiarelli G, Nottola SA, Vizza E, Correr S, Motta PM. Changes of ovarian microvasculature in hCG stimulated rabbits. A scanning electron microscopic study of corrosion casts. Ital J Anat Embryol 1995;100:469–77.
[9] Macchiarelli G, Nottola SA, Picucci K, Stallone T, Motta PM. The microvasculature of the corpus luteum in pregnant rabbit. A scanning electron microscopy study of corrosion casts. Ital J Anat Embryol 1998;103:191–202.
[10] Nottola SA, Macchiarelli G, Motta PM. The angioarchitecture of estrous, pseudopregnant and pregnant rabbit ovary as seen by scanning electron microscopy of vascular corrosion casts. Cell Tissue Res 1997;288:353–63.
[11] Fraser HM, Wulff C. Angiogenesis in the corpus luteum. Reprod Biol Endocrinol 2003;1:88.
[12] Acosta TJ, Hayashi KG, Ohtani M, Miyamoto A. Local changes in blood flow within the preovulatory follicle wall and early corpus luteum in cows. Reproduction 2003;125:759–67.
[13] Redmer DA, Reynolds LP. Angiogenesis in the ovary. Rev Reprod 1996;1:182–92.
[14] Redmer DA, Doraiswamy V, Bortnem BJ, Fisher K, Jablonka-Shariff A, Grazul-Bilska AT, et al. Evidence for a role of capillary pericytes in vascular growth of the developing ovine corpus luteum. Biol Reprod 2001;65:879–89.
[15] Robinson RS, Woad KJ, Hammond AJ, Laird M, Hunter MG, Mann GE. Angiogenesis and vascular function in the ovary. Reproduction 2009;138:869–81.
[16] Bukovsky A. Immune maintenance of self in morphostasis of distinct tissues, tumour growth and regenerative medicine. Scand J Immunol 2011;73:159–89.
[17] Reisinger K, Baal N, McKinnon T, Münstedt K, Zygmunt M. The gonadotropins: tissue-specific angiogenic factors? Mol Cell Endocrinol 2007;269:65–80.
[18] Ribeiro LA, Bacci ML, Seren E, Tamanini C, Forni M. Characterization and differential expression of vascular endothelial growth factor isoforms and receptors in swine corpus luteum throughout estrous cycle. Mol Reprod Dev 2007;74:163–71.
[19] Jiang JY, Miyabayashi K, Nottola SA, Umezu M, Cecconi S, Sato E, et al. Thyroxine treatment stimulated ovarian follicular angiogenesis in immature hypothyroid rats. Histol Histopathol 2008;23:1387–98.
[20] Hosoda Y, Sasaki N, Agui T. Female infertility in grt mice is caused by thyroid hormone deficiency, not by insufficient TPST2 activity in the reproductive organs. J Vet Med Sci 2008;70:1043–9.
[21] Maruo T, Katayama K, Barnea ER, Mochizuki M. A role for thyroid hormone in the induction of ovulation and corpus luteum function. Horm Res 1992;37:12–8.
[22] Abalovich M, Mitelberg L, Allami C, Gutierrez S, Alcaraz G, Otero P, et al. Subclinical hypothyroidism and thyroid autoimmunity in women with infertility. Gynecol Endocrinol 2007;23:279–83.
[23] Hagino N. Influence of hypothyroid state on ovulation in rats. Endocrinology 1971;88:1332–6.
[24] Jiang JY, Miyoshi K, Umezu M, Sato E. Superovulation of immature hypothyroid rdw rats by thyroxine therapy and the development of eggs after in vitro fertilization. J Reprod Fertil 1999;116:19–24.
[25] Jiang JY, Umezu M, Sato E. Improvement of follicular development rather than gonadotrophin secretion by thyroxine treatment in infertile immature hypothyroid rdw rats. J Reprod Fertil 2000;119: 193–9.
[26] Tomanek RJ, Doty MK, Sandra A. Early coronary angiogenesis in response to thyroxine: growth characteristics and upregulation of basic fibroblast growth factor. Circ Res 1998;82:587–93.

[27] Liu Y, Wang D, Redetzke RA, Sherer BA, Gerdes AM. Thyroid hormone analog 3,5-diiodothyropropionic acid promotes healthy vasculature in the adult myocardium independent of thyroid effects on cardiac function. Am J Physiol Heart Circ Physiol 2009;296:1551–7.
[28] Zhang L, Cooper-Kuhn CM, Nannmark U, Blomgren K, Kuhn HG. Stimulatory effects of thyroid hormone on brain angiogenesis in vivo and in vitro. J Cereb Blood Flow Metab 2010;30:323–35.
[29] Davis PJ, Davis FB, Mousa SA, Luidens MK, Lin HY. Membrane receptor for thyroid hormone: physiologic and pharmacologic implications. Annu Rev Pharmacol Toxicol 2011;51:99–115.
[30] Luidens MK, Mousa SA, Davis FB, Lin HY, Davis PJ. Thyroid hormone and angiogenesis. Vascul Pharmacol 2010;52:142–5.
[31] Jiang JY, Imai Y, Umezu M, Sato E. Characteristics of infertility in female hypothyroid (hyt) mice. Reproduction 2001;122:695–700.
[32] Reynolds LP, Redmer DA. Expression of the angiogenic factors, basic fibroblast growth factor and vascular endothelial growth factor, in the ovary. J Anim Sci 1998;76:1671–81.
[33] Martelli A, Palmerini MG, Russo V, Rinaldi C, Bernabò N, Di Giacinto O, et al. Blood vessel remodeling in pig ovarian follicles during the periovulatory period: an immunohistochemistry and SEM-corrosion casting study. Reprod Biol Endocrinol 2009;7:72.
[34] Jiang JY, Macchiarelli G, Tsang BK, Sato E. Capillary angiogenesis and degeneration in bovine ovarian antral follicles. Reproduction 2003; 125:211–23.
[35] Tilton RG, LaRose LS, Kilo C, Williamson JR. Absence of degenerative changes in retinal and uveal capillary pericytes in diabetic rats. Invest Ophthalmol Vis Sci 1986;27:716–21.
[36] Motta PM, Nottola SA, Familiari G, Makabe S, Stallone T, Macchiarelli G. Morphodynamics of the follicular-luteal complex during early ovarian development and reproductive life. Int Rev Cytol 2003;223:177–288.
[37] Murakami T. Application of the scanning electron microscope to the study of the fine distribution of the blood vessels. Arch Histol Cytol 1971;32:445–54.
[38] Sato E, Jiang JY. Follicular development and ovulation in hypothyroid rdw rats. Ital J Anat Embryol 2001;106:249–56.
[39] Macchiarelli G, Vizza E, Nottola SA, Familiari G, Motta PM. Cellular and microvascular changes of the ovarian follicle during folliculogenesis: a scanning electron microscopic study. Arch Histol Cytol 1992;55:191–204.
[40] Fraser HM, Duncan WC. SRB Reproduction, Fertility and Development Award Lecture 2008. Regulation and manipulation of angiogenesis in the ovary and endometrium. Reprod Fertil Dev 2009;21: 377–92.
[41] Maruo T, Hayashi M, Matsuo H, Yamamoto T, Okada H, Mochizuki M. The role of thyroid hormone as a biological amplifier of the actions of follicle-stimulating hormone in the functional differentiation of cultured porcine granulosa cells. Endocrinology 1987;121:1233–41.
[42] Wakim AN, Polizotto SL, Burholt DR. Augmentation by thyroxine of human granulosa cell gonadotrophin-induced steroidogenesis. Hum Reprod 1995;10:2845–8.
[43] Cecconi S, Rucci N, Scaldaferri ML, Masciulli MP, Rossi G, Moretti C, et al. Thyroid hormone effects on mouse oocyte maturation and granulosa cell aromatase activity. Endocrinology 1999;140:1783–8.
[44] Aghajanova L, Lindeberg M, Carlsson IB, Stavreus-Evers A, Zhang P, Scott JE, et al. Receptors for thyroid-stimulating hormone and thyroid hormones in human ovarian tissue. Reprod Biomed Online 2009;18:337–47.
[45] Bergh JJ, Lin HY, Lansing L, Mohamed SN, Davis FB, Mousa S, et al. Integrin alphaVbeta3 contains a cell surface receptor site for thyroid hormone that is linked to activation of mitogen-activated protein kinase and induction of angiogenesis. Endocrinology 2005;146: 2864–71.
[46] Stratman AN, Malotte KM, Mahan RD, Davis MJ, Davis GE. Pericyte recruitment during vasculogenic tube assembly stimulates endothelial basement membrane matrix formation. Blood 2008;114: 5091–101.
[47] Silva R, D'Amico G, Hodivala-Dilke KM, Reynolds LE. Integrins. The keys to unlocking angiogenesis. Arterioscler Thromb Vasc Biol 2008; 28:1703–13.
[48] Somanatah PR, Ciocea A, Byzova TV. Integrin and growth factor receptor alliance in angiogenesis. Cell Biochem Biophys 2009;53: 53–64.
[49] Sleer LS, Taylor CC. Platelet-derived growth factors and receptors in the rat corpus luteum: localization and identification of an effect on luteogenesis. Biol Reprod 2007;76:391–400.
[50] Armulik A, Genové G, Betsholtz C. Pericytes: developmental, physiological, and pathological perspectives, problems, and promises. Dev Cell 2011;21:193–215.
[51] Ribatti D, Nico B, Crivellato E. The role of pericytes in angiogenesis. Reprod Biol Endocrinol 2011;55:261–8.
[52] Woad KJ, Hammond AJ, Hunter M, Mann GE, Hunter MG, Robinson RS. FGF2 is crucial for the development of bovine luteal endothelial networks in vitro. Reproduction 2009;138:581–8.
[53] Wulff C, Dickson SE, Duncan WC, Fraser HM. Angiogenesis in the human corpus luteum: simulated early pregnancy by HCG treatment is associated with both angiogenesis and vessel stabilization. Hum Reprod 2001;16:2515–24.
[54] Berisha B, Schams D, Kosmann M, Amselgruber W, Einspanier R. Expression and tissue concentration of vascular endothelial growth factor, its receptors, and localization in the bovine corpus luteum during estrous cycle and pregnancy. Biol Reprod 2000;63:1106–14.
[55] Fraser HM, Bell J, Wilson H, Taylor PD, Morgan K, Anderson RA, et al. Localization and quantification of cyclic changes in the expression of endocrine gland vascular endothelial growth factor in the human corpus luteum. J Clin Endocrinol Metab 2005;90:427–34.
[56] van den Driesche S, Myers M, Gay E, Thong KJ, Duncan WC. HCG up-regulates hypoxia inducible factor-1 alpha in luteinized granulosa cells: implications for the hormonal regulation of vascular endothelial growth factor A in the human corpus luteum. Mol Hum Reprod 2008;14:455–64.
[57] Gerber HP, Dixit V, Ferrara N. Vascular endothelial growth factor induces expression of the antiapoptotic proteins Bcl-2 and A1 in vascular endothelial cells. J Biol Chem 1998;273:13313–6.
[58] Grazul-Bilska AT, Redmer DA, Jablonka-Shariff A, Biondini ME, Reynolds LP. Proliferation and progesterone production of ovine luteal cells from several stages of the estrous cycle: effects of fibroblast growth factors and luteinizing hormone. Can J Physiol Pharmacol 1995;73:491–500.
[59] Woad KJ, Hunter MG, Mann GE, Laird M, Hammond AJ, Robinson RS. Fibroblast growth factor 2 is a key determinant of vascular sprouting during bovine luteal angiogenesis. Reproduction 2012; 143:35–43.
[60] Yamashita H, Kamada D, Shirasuna K, Matsui M, Shimizu T, Kida K, et al. Effect of local neutralization of basic fibroblast growth factor or vascular endothelial growth factor by a specific antibody on the development of the corpus luteum in the cow. Mol Reprod Dev 2008;75:1449–56.
[61] Sriperumbudur R, Zorrilla L, Gadsby JE. Transforming growth factor-beta (TGFbeta) and its signaling components in peri-ovulatory pig follicles. Anim Reprod Sci 2010;120:84–94.
[62] Zamah AM, Hsieh M, Chen J, Vigne JL, Rosen MP, Cedars MI, et al. Human oocyte maturation is dependent on LH-stimulated accumulation of the epidermal growth factor-like growth factor, amphiregulin. Hum Reprod 2010;25:2569–78.
[63] Huber AV, Saleh L, Prast J, Haslinger P, Knöfler M. Human chorionic gonadotrophin attenuates NF-kappaB activation and cytokine expression of endometriotic stromal cells. Mol Hum Reprod 2007; 13:595–604.
[64] Cecconi S, Rossi G, Coticchio G, Macchiarelli G, Borini A, Canipari R. Influence of thyroid hormone on mouse preantral follicle development in vitro. Fertil Steril 2004;81(Suppl 1):919–24.
[65] Kikuta A, Macchiarelli G, Murakami T. Microvasculature of the ovary. In: Motta PM, editor. Ultrastructure of the ovary. Boston: Kluwer Academic Publishers; 1991. p. 239–54.

Zygote: page 1 of 7 © Cambridge University Press 2012
doi:10.1017/S0967199412000469

Distribution of tubulointerstitial nephritis antigen-like 1 and structural matrix proteins in mouse embryos during preimplantation development *in vivo* and *in vitro*

Masahiro Sakurai[1,2], *Yusuke Sato*[2], *Kuniaki Mukai*[3], *Makoto Suematsu*[3], *Emiko Fukui*[4], *Midori Yoshizawa*[4], *Kentaro Tanemura*[2], *Yumi Hoshino*[2], *Hiromichi Matsumoto*[2,4] *and Eimei Sato*[2]

Laboratory of Animal Reproduction, Graduate School of Agricultural Science, Tohoku University, Sendai, Japan; Department of Biochemistry, School of Medicine, Keio University, Tokyo, Japan; and Laboratory of Animal Breeding and Reproduction, Faculty of Agriculture, Utsunomiya University, Tochigi, Japan

Date submitted: 21.04.2012. Date revised: 15.06.2012. Date accepted: 22.06.2012

Summary

Tubulointerstitial nephritis antigen-like 1 (TINAGL1) is a novel matricellular protein that interacts with structural matrix proteins and promotes cell adhesion and spreading. We have previously reported unique localization of TINAGL1 to the trophectoderm (TE) of mouse blastocysts. TINAGL1 was found to be upregulated in implantation-competent blastocysts after estrogen treatment using progesterone-treated delayed-implantation models. Moreover, colocalization of TINAGL1 and extracellular matrix (ECM) protein laminin 1 was detected in the Reichert membrane on embryonic days 6.5 and 7.5. Although these data suggested a role for TINAGL1 in the embryo development at postimplantation, its relevance to other ECM proteins during preimplantation development is not clear. In this study, we examined the expression of TINAGL1 and its relevance to other ECM proteins fibronectin (FN) and collagen type IV (ColIV) during *in vivo* development of preimplantation embryos, particularly at blastocyst stage in detail. Localizations of TINAGL1, FN, and ColIV were similar. In 1-cell to 8-cell embryos, they were expressed in cytoplasm of blastomeres, and in morulae they were localized in the outer cells. FN and ColIV were expressed primarily on outer surface of the cells. In blastocysts, FN and ColIV were distributed in the cytoplasm of TE, but, just prior to implantation, they became localized uniquely to the blastocoelic surface of TE. In *in vitro* fertilized (IVF) blastocysts, expression levels of TINAGL1 and FN were lower than in *in vivo* blastocysts. These results suggest that, during preimplantation development, TINAGL1 may be involved in roles of structural matrix proteins, whose expression in blastocysts may be affected by *in vitro* culture.

Keywords: Collagen Type IV, Fibronectin, Preimplantation development, TINAGL1, Trophectoderm

Introduction

The fertilized oocyte first undergoes a series of early cleavage divisions to produce increasing numbers of progressively smaller cells, known as blastomeres, without changing the overall size of the embryo; it spans compaction and morula formation, and finally, cavitation with formation of a blastocyst. During mouse preimplantation embryo development, the 1-cell embryo develops into a blastocyst, a process that takes 4 days. In the mouse, the first sign of the attachment reaction (apposition stage) in the process of implantation occurs in the evening on day 4 of pregnancy (day 1 = vaginal plug) (Dey *et al.*, 2004; Wang & Dey, 2006). Estrogen secretion around noon on day 4 of pregnancy is essential for on-time blastocyst activation for implantation (Yoshinaga & Adams, 1966; Paria *et al.*, 1993). However, the mechanisms that regulate preimplantation embryo development are not fully understood.

Tubulointerstitial nephritis antigen-like 1 (TINAGL1; also known as adrenocortical zonation factor

[1]All correspondence to: Masahiro Sakurai. Laboratory of Animal Reproduction, Graduate School of Agricultural Science, Tohoku University, Sendai, 981-8555, Japan. Tel:/Fax: +81 22 717 8687. e-mail: msaku913@affrc.go.jp
[2]Laboratory of Animal Reproduction, Graduate School of Agricultural Science, Tohoku University, 1-1 Amamiya-machi, Tsutsumidori, Aoba-ku, Sendai, Miyagi, 981-8555, Japan.
[3]Department of Biochemistry, School of Medicine, Keio University, 35 Shinano-machi, Shinjuku-ku, Tokyo, 160-8582, Japan.
[4]Laboratory of Animal Breeding and Reproduction, Faculty of Agriculture, Utsunomiya University, 350 Mine-machi, Utsunomiya, Tochigi, 321-8505, Japan.

1 [AZ-1] or lipocalin 7) is a secretory protein of 52 kD polypeptides that was cloned from mouse adrenocortical cells and is known to be closely associated with the zonal differentiation of adrenocortical cells (Mukai *et al.*, 2003). Recently, we demonstrated the expression and localization of TINAGL1 in peri-implantation mouse embryos (Igarashi *et al.*, 2009). Just prior to implantation at 23:00 h on day 4 of pregnancy, TINAGL1 was uniquely distributed in the blastocysts. Specifically, TINAGL1 was localized to the blastocoel site surface of the trophectoderm (TE) in implantation-competent (activated) blastocysts. This blastocyst activation can be initiated rapidly by a single injection of estradiol-17β (E_2) into ovariectomized and progesterone-primed pregnant mice, and is known as the delayed-implantation model (Yoshinaga & Adams, 1966; Psychoyos, 1973). In fact, we have also demonstrated the same localization and increased expression of TINAGL1 in activated blastocysts after E_2 treatment using this mouse model (Igarashi *et al.*, 2009). This unique localization may indicate a physiological role for TINAGL1 in the preparation of the blastocyst for successful implantation and/or subsequent pregnancy. We also demonstrated that, at postimplantation, TINAGL1 is a novel component of the Reichert membrane and interacts with laminin (LN) 1, and most likely plays a physical and physiological role in embryo development (Igarashi *et al.*, 2009). However, the relationship between TINAGL1 and other structural extracellular matrix (ECM) molecules in the mouse embryo, including fibronectin (FN) and collagen type IV (ColIV), is not clear.

ECM is present in every tissue but is most highly enriched in connective tissue and basement membrane (BM). ECM provides physical support to tissues and organs by occupying the space between cells. FN is a major constituent of ECM that promotes cell adhesion, spreading migration, and cytoskeletal organization (Hynes, 1990). ColIV is largely considered to be a structural component of BM, where it forms a scaffold with which other BM components, such as LN or FN, can associate (Laurie *et al.*, 1986), and it also mediates various cell functions directly (Murray *et al.*, 1979; Rubin *et al.*, 1981; Aumailley & Timpl, 1986). Some *in vitro* experiments suggest that FN promotes trophoblast adhesion, which may restrict migration, while other studies indicate that it facilitates motility (Burrows *et al.*, 1993; Damsky *et al.*, 1994; Irving *et al.*, 1995; Stephens *et al.*, 1995; Yelian *et al.*, 1995). ColIV can also support the outgrowth of primary trophoblast from the mouse blastocyst (Armant *et al.*, 1986; Sutherland *et al.*, 1988). Although some investigations into the expression of FN (Zetter & Martin, 1978; Wartiovaara *et al.*, 1979; Yohkaichiya *et al.*, 1988) and ColIV (Leivo *et al.*, 1980; Sherman *et al.*, 1980) in preimplantation embryos have been performed, detailed analyses of their expression from blastocyst activation to just prior to implantation have not been conducted.

In this study, we compared the immunocytological distributions of TINAGL1, FN, and ColIV during mouse preimplantation development, particularly in blastocysts at three stages: (1) before estrogen secretion; (2) after estrogen secretion; and (3) just prior to implantation. Importantly, it is known that *in vitro* culture (IVC) of preimplantation embryos alters their global gene expression patterns (Rinaudo & Schultz, 2004; Rinaudo *et al.*, 2006) and affects the behavior of mice after birth (Ecker *et al.*, 2004; Fernandez-Gonzalez *et al.*, 2004). Therefore, we compared further their expression in *in vivo* and *in vitro* fertilized (IVF) blastocysts.

Materials and methods

Animals

All ICR mice were purchased from Japan SLC Inc. (Shizuoka, Japan), and housed under controlled temperatures (22–27°C) with a constant photoperiod (13L–11D). Mice were provided with a pelleted diet (Oriental Yeast Co. Ltd., Japan) and water *ad libitum*. All investigations were performed in accordance with the Guide for Care and Use of Laboratory Animals of the Graduate School of Agricultural Science, Tohoku University.

In vivo embryo collection

Preimplantation embryos were collected as described previously (Igarashi *et al.*, 2009). In brief, female mature mice were mated with fertile males to induce pregnancy (day 1 [10:00 h] = vaginal plug). Removed oviducts or uteri were flushed with Ca^{2+}- and Mg^{2+}-free Dulbecco's phosphate-buffered saline (PBS, Nissui Pharmaceutical Co., Ltd., Japan) containing 0.1% polyvinyl alcohol (PVA, Sigma). Preimplantation embryos were collected at the following stages during pregnancy: 1-cell, 2-cell, 4-cell, 8-cell, morula, and blastocyst on days 1 (21:00 h), 2 (10:00 h), 3 (01:00 h), 3 (10:00 h), 3 (21:00 h), and 4 (10:00 [before estrogen secretion], 18:00 [after estrogen secretion], and 23:00 h [just prior to implantation]), respectively.

In vitro fertilization and embryo culture

In vitro fertilization and embryo culture were performed as described previously (Matsumoto *et al.*, 2001; Hoshino & Sato, 152 2008). Immature mice were superovulated by subcutaneous injection with 5 IU of pregnant mare serum gonadotropin (PMSG;

ASKA Pharmaceutical Co., Ltd, Japan) at 3 weeks of age, followed by injection of 5 IU of human chorionic gonadotropin (hCG; Yell Pharmaceutical Co., Ltd, Japan) 48 h later. Mice were killed by cervical dislocation and oviducts were removed at 14 h post-hCG injection. Mature male mice over 8 weeks of age were killed by cervical dislocation and the epididymis was removed and carefully blotted free of blood and adipose tissues. Cauda epididymis was cut with fine scissors and the sperm droplet was scooped out with a 26-gauge needle (Terumo Co., Japan) and immediately transferred to a 200 μl drop of human tubal fluid (HTF) medium covered with mineral oil (Nacalai Tesque, Japan). Capacitation was allowed to proceed for 2–3 h at 37 °C in 5% CO_2 in humidified air. Collected cumulus cell–oocyte complexes (COCs) were moved to the HTF medium; the final concentration was 700 spermatozoa/μl. At 4 h after insemination, oocytes were cultured in a 100 μl drop of potassium simplex optimized medium (KSOM) overlaid with mineral oil in a humidified atmosphere of 5% CO_2 in air at 37°C. At 120 and 144 h after embryo culture, blastocysts were collected for immunostaining or western blotting.

Blastocyst stage developed *in vivo* and *in vitro*

Animal studies using the mouse model have demonstrated that after blastocoel formation in the morning on day 4 of pregnancy, the blastocysts are activated *in utero* around noon of day 4 for successful implantation to occur (Paria *et al.*, 1993), when an estrogen secretion takes place (Nilsson, 1966). Furthermore, just prior to implantation, activated blastocysts have a morphologically distinct structure (reviewed in ref. (McRae & Church, 1990)). In this study, the typical stages of *in vivo* blastocysts were as follows: pre-expansion (at 10:00 h before estrogen secretion); from expanded to hatched (at 18:00 h after estrogen secretion, referred to below as peri-hatching); and implantation-competent (at 23:00 h just prior to implantation, defined below as activated). In contrast, we collected IVF blastocysts following embryo culture for 120 or 144 h, because their most typical stages at each time point were pre-expansion or peri-hatching.

Immunostaining of embryos

Immunostaining of preimplantation embryos was performed as described previously (Matsumoto *et al.*, 2004; Li *et al.*, 2007; Igarashi *et al.*, 2009), with slight modifications. In brief, preimplantation embryos were fixed in 3.7% formaldehyde (Wako Pure Chemical Industries, Ltd., Japan) in PBS containing 0.1% PVA at room temperature for 30 min, and permeabilized with 0.25% Triton X-100 (Wako) in PBS containing 0.1% PVA for 5 min. After washing three times with PBS containing 0.1% PVA, embryos were incubated with rabbit anti-TINAGL1 polyclonal antibody (diluted 1:200), which was prepared as described previously (Li *et al.*, 2007), rabbit anti-fibronectin polyclonal antibody (diluted 1:50; Sigma), or rabbit anti-collagen type IV polyclonal antibody (diluted 1:50; Chemicon) overnight at 4°C. Following washes three times with PBS containing 0.25% Triton X-100 and 0.1% PVA, embryos were incubated with Alexa Fluor 488 goat anti-rabbit IgG (dilution 1:200, Invitrogen) for 1 h at room temperature. Washed three times with PBS containing 0.25% Triton X-100 and 0.1% PVA, nuclei were labelled with 10 μg/ml propidium iodide (Sigma) for 1 h at room temperature. After three washes, embryos were viewed using a Bio-Rad MRC-1024 confocal scanning laser microscope mounted on an Axioplan Zeiss microscope.

Western blotting

Western blot analysis was performed as described previously (Igarashi *et al.*, 2009). In brief, collected blastocysts were solubilized in 2× SDS sample buffer (0.5M Tris–HCl [Sigma] at pH 6.8, 10% β-mercaptoethanol [Wako], and 20% glycerol [Wako]). Electrophoresis was performed with 50 blastocysts in each lane on 12% polyacrylamide gels, and the resolved proteins were transferred to polyvinylidene fluoride (PVDF) membranes (Millipore Corporate Headquarters, MA). Thereafter, the membranes were blocked for 1 h at room temperature with Tris-buffered saline (TBS) containing 0.1% Tween 20 (Wako) (TBS-T) and 5% skimmed milk (Wako). Membranes were next incubated with rabbit anti-TINAGL1 polyclonal antibody (diluted 1:2000) overnight at 4 °C. Then, the membranes were reacted with horseradish peroxidase-conjugated goat anti-rabbit IgG (diluted 1:40,000) for 1 h at room temperature. Peroxidase activity was visualized using the ECL Plus western blotting detection system (GE Healthcare, Ltd., UK).

Results

Distribution of TINAGL1, FN, and ColIV in 1-cell embryos to morulae

To compare the cellular localization of TINAGL1 with that of FN and ColIV in preimplantation embryos, immunostaining was performed. In 1-cell to 8-cell embryos before compaction, TINAGL1 was localized in the cytoplasm. However, in compacted morulae, TINAGL1 was primarily localized in the outer cells. FN and ColIV were also expressed in the cytoplasm, but were more strongly distributed on the outer surface of the blastomeres than in the cytoplasm in

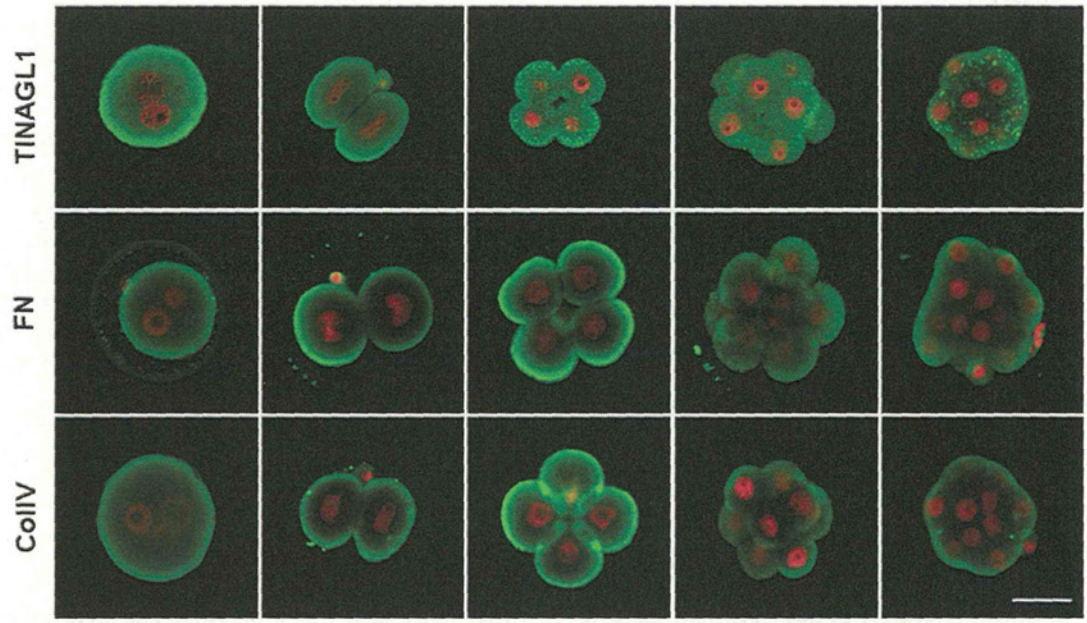

Figure 1 Distribution of TINAGL1, FN, and ColIV in 1-cell embryo to morula. Collected *in vivo* embryos (1-, 2-, 4- and 8-cell embryos, and compacted morulae) were immunostained for each protein with Alexa Fluor 488 (green). Red shows nuclei. Upper panel: TINAGL1. Middle panel: FN. Lower panel: ColIV. Bar = 50 μm. (See online for a colour version of this figure.)

1-cell to 8-cell embryos. In morulae, TINAGL1, FN, and ColIV were expressed in the outer cells (Fig. 1).

Distribution of TINAGL1, FN, and ColIV in blastocysts

In blastocysts, TINAGL1 was expressed in the cytoplasm of TE cells before (10:00 h) and after (18:00 h) estrogen secretion. Importantly, just prior to implantation (23:00 h), the distribution of TINAGL1 changed from the cytoplasm to the inner (blastocoelic) surface of TE cells. Similar to TINAGL1, FN and ColIV were also localized in the cytoplasm of TE in blastocysts before and after estrogen secretion. Just prior to implantation, their distribution patterns changed and they were localized mainly at the inner surface of TE. ColIV was also expressed in the cytoplasm of the inner cell mass (ICM) (Fig. 2).

Expression level of TINAGL1 in blastocyst developed *in vivo* and *in vitro*

As shown in Fig. 3, the expression of TINAGL1 in IVF blastocysts after 120 h of embryo culture was lower than that in *in vivo* blastocysts at 10:00 h, indicating that the expression of TINAGL1 in blastocysts at pre-expansion stage was lower in IVF than in *in vivo* blastocysts. Thereafter, the expression increased in both *in vivo* and IVF blastocysts (at 23:00 h in *in vivo* blastocysts and at 144 h in IVF blastocysts).

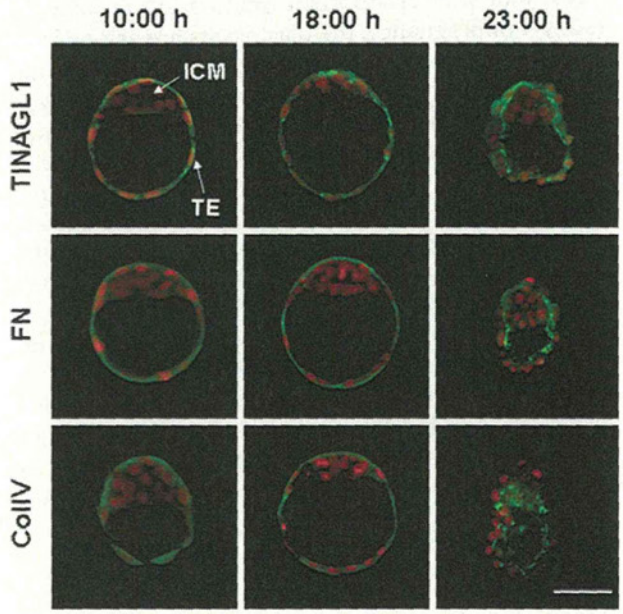

Figure 2 Distribution of TINAGL1, FN, and ColIV in mouse blastocyst. *In vivo* blastocysts were collected at 10:00 h (before estrogen secretion), 18:00 h (after estrogen secretion), and 23:00 h (just prior to implantation) on day 4 of pregnancy and immunostained for each protein with Alexa Fluor 488 (green). Red shows nuclei. Upper panel: TINAGL1. Middle panel: FN. Lower panel: ColIV. ICM: inner cell mass. TE: trophectoderm. Bar = 50 μm. (See online for a colour version of this figure.)

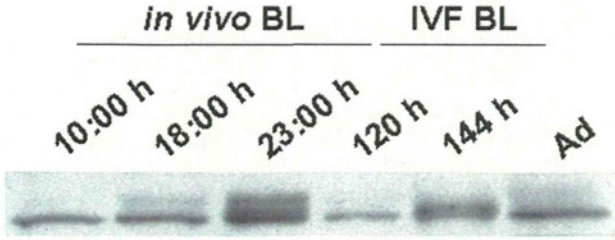

Figure 3 Expression of TINAGL1 in mouse blastocyst. *In vivo* blastocysts (BL) were collected at 10:00 h, 18:00 h, and 23:00 h on day 4 of pregnancy. IVF blastocysts were collected at 120 h and 144 h after embryo culture. Ad: adrenal gland as positive control expressing TINAGL1.

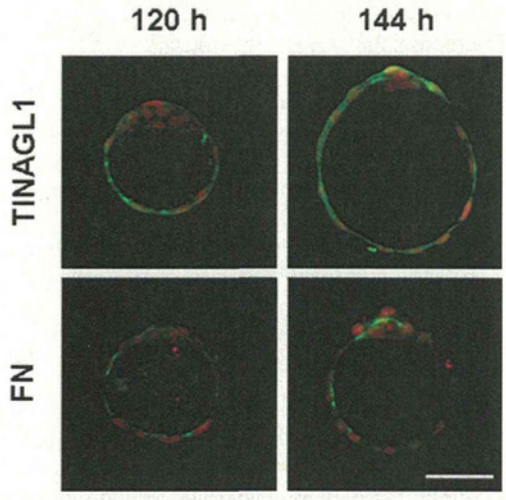

Figure 4 Distribution of TINAGL1 and FN in mouse IVF blastocyst. IVF blastocysts collected at 120 or 144 h after embryo culture were immunostained for each protein with Alexa Fluor 488 (green). Red shows nuclei. Upper panel: TINAGL1. Lower panel: FN. Bar = 50 μm. (See online for a colour version of this figure.)

Distribution of TINAGL1 and FN in IVF blastocysts

TINAGL1 and FN were localized in the cytoplasm of TE cells in IVF blastocysts (Fig. 4). Immunostaining showed that the expression of FN in IVF blastocysts was lower than that in *in vivo* blastocysts (refer Fig. 2, middle panel).

Discussion

In blastocysts, the localizations of FN and ColIV were similar to that of TINAGL1 in the TE, except for the strong expression of ColIV in the ICM. Importantly, these three proteins were distributed at the blastocoelic surface of the TE just prior to implantation. It is known that the TE secretes a BM; several molecules have been localized to the TE-generated BM, including FN, LN, ColIV, and heparin sulfate proteoglycans (Wartiovaara *et al.*, 1979; Leivo *et al.*, 1980; Carnegie, 1991; Thorsteinsdottir, 1992; Hierck *et al.*, 1993; Salamat *et al.*, 1993). *In vitro* outgrowth assays have demonstrated that the cellular attachment and outward migration were activated on FN (Bartlett & Menino, 1995; Schilperoort-Haun & Menino, 2002a,b) and, to a greater extent, on ColIV (Carnegie & Cabaca, 1991, 1993) in several species. It has been suggested that, upon secretion, TINAGL1 immediately binds to the ECM proximal to the secreting cells or their cell surface receptors, and promotes the adhesion of adrenocortical cells in an autocrine or paracrine manner through interaction with cell surface integrin receptors (Li *et al.*, 2007). In addition, TINAGL1 immobilized on a substratum or bound to FN or collagen promoted adhesion and spreading of adrenocortical cells (Li *et al.*, 2007). In our previous report, we showed that another structural matrix protein, LN1, was not distributed at the blastocoelic surface of the TE and did not colocalize with TINAGL1 at 23:00 h on day 4 of pregnancy (Igarashi *et al.*, 2009). Taken all together, it is conceivable that, just prior to implantation, TINAGL1 secreted from the TE may be involved in some roles of TE-generated BM composed of FN and ColIV, but not LN1, at the blastocoelic surface.

One of the major problems with IVF today is the low pregnancy rate after successful embryo transfer due to implantation failure or early embryonic loss. The fact that growth factor-soaked beads transferred into the uterus of pseudopregnant mice efficiently elicited discrete local implantation-like responses, such as increased vascular permeability, decidualization, and expression of implantation marker genes (Paria *et al.*, 2001), indicates that the low pregnancy rate is attributed to the embryos rather than the uterus. Furthermore, different gene expression patterns between *in vivo* and IVF embryos have been observed (Rinaudo & Schultz, 2004; Rinaudo *et al.*, 2006). In this study, the distributions of TINAGL1 and FN were the same in IVF blastocysts and *in vivo* blastocysts, except that their expressions were low in IVF blastocysts. These data are in accordance with a previous report showing that *in vivo*-derived bovine blastocysts exhibited a 2.64-fold increase in FN expression compared with IVF blastocysts (Mohan *et al.*, 2004). Moreover, in the mouse, it was reported that the expression of *procollagen, type IV alpha 1* mRNAs was 0.60-fold lower in IVF blastocysts than in *in vivo* blastocysts (Giritharan *et al.*, 2007), and immunostaining for ColIV showed that IVF blastocysts contained poorly developed ECM (Summers *et al.*, 2000).

From this study, the following hypothesis is inferred. Low expression levels of ECM proteins, such as FN and ColIV, and supporting molecules, which may

include TINAGL1, during blastocyst formation *in vitro* may affect subsequent postimplantation embryonic development.

Acknowledgements

This work was supported by the Japan Society for the Promotion of Science Grant to E. Sato (No. 21248032).

References

Armant, D.R., Kaplan, H.A. & Lennarz, W.J. (1986). Fibronectin and laminin promote *in vitro* attachment and outgrowth of mouse blastocysts. *Dev. Biol.* **116**, 519–23.

Aumailley, M. & Timpl, R. (1986). Attachment of cells to basement membrane collagen type IV. *J. Cell Biol.* **103**, 1569–75.

Bartlett, S.E. & Menino, A.R., Jr (1995). Evaluation of extracellular matrices and the plasminogen activator system in sheep inner cell mass and trophectodermal outgrowth *in vitro*. *Biol. Reprod.* **52**, 1436–45.

Burrows, T.D., King, A. & Loke, Y.W. (1993). Expression of integrins by human trophoblast and differential adhesion to laminin or fibronectin. *Hum. Reprod.* (Oxford, England) **8**, 475–84.

Carnegie, J.A. (1991). Immunolocalization of fibronectin and laminin within rat blastocysts cultured under serum-free conditions. *J. Reprod. Fertil.* **91**, 423–34.

Carnegie, J.A. & Cabaca, O. (1991). The influence of extracellular matrix components on the proliferation and migration of inner cell mass-derived parietal endodermal cells. *Biol. Reprod.* **45**, 572–80.

Carnegie, J.A. & Cabaca, O. (1993). Extracellular matrix composition and resilience: two parameters that influence the *in vitro* migration and morphology of rat inner cell mass-derived cells. *Biol. Reprod.* **48**, 287–99.

Damsky, C.H., Librach, C., Lim, K.H., Fitzgerald, M.L., McMaster, M.T., Janatpour, M., Zhou, Y., Logan, S.K. & Fisher, S.J. (1994). Integrin switching regulates normal trophoblast invasion. *Development* (Cambridge, England) **120**, 3657–66.

Dey, S.K., Lim, H., Das, S.K., Reese, J., Paria, B.C., Daikoku, T. & Wang, H. (2004). Molecular cues to implantation. *Endocrine Rev.* **25**, 341–73.

Ecker, D.J., Stein, P., Xu, Z., Williams, C.J., Kopf, G.S., Bilker, W.B., Abel, T. & Schultz, R.M. (2004). Long-term effects of culture of preimplantation mouse embryos on behavior. *Proc. Natl. Acad. Sci. USA* **101**, 1595–600.

Fernandez-Gonzalez, R., Moreira, P., Bilbao, A., Jimenez, A., Perez-Crespo, M., Ramirez, M.A., Rodriguez De Fonseca, F., Pintado, B. & Gutierrez-Adan, A. (2004). Long-term effect of *in vitro* culture of mouse embryos with serum on mRNA expression of imprinting genes, development, and behavior. *Proc. Natl. Acad. Sci. USA* **101**, 5880–5.

Giritharan, G., Talbi, S., Donjacour, A., Di Sebastiano, F., Dobson, A.T. & Rinaudo, P.F. (2007). Effect of *in vitro* fertilization on gene expression and development of mouse preimplantation embryos. *Reproduction* (Cambridge, England), **134**, 63–72.

Hierck, B.P., Thorsteinsdottir, S., Niessen, C.M., Freund, E., Iperen, L.V., Feyen, A., Hogervorst, F., Poelmann, R.E., Mummery, C.L. & Sonnenberg, A. (1993). Variants of the alpha 6 beta 1 laminin receptor in early murine development: distribution, molecular cloning and chromosomal localization of the mouse integrin alpha 6 subunit. *Cell Adhes. Commun.* 1, 33–53.

Hoshino, Y. & Sato, E. (2008). Protein kinase B (PKB/Akt) is required for the completion of meiosis in mouse oocytes. *Dev. Biol.* **314**, 215–23.

Hynes, R.O. (1990). *Fibronectins*, New York: Springer-Verlag.

Igarashi, T., Tajiri, Y., Sakurai, M., Sato, E., Li, D., Mukai, K., Suematsu, M., Fukui, E., Yoshizawa, M. & Matsumoto, H. (2009). Tubulointerstitial nephritis antigen-like 1 is expressed in extraembryonic tissues and interacts with laminin 1 in the Reichert membrane at postimplantation in the mouse. *Biol. Reprod.* **81**, 948–55.

Irving, J.A., Lysiak, J.J., Graham, C.H., Hearn, S., Han, V.K. & Lala, P.K. (1995). Characteristics of trophoblast cells migrating from first trimester chorionic villus explants and propagated in culture. *Placenta* **16**, 413–33.

Laurie, G.W., Bing, J.T., Kleinman, H.K., Hassell, J.R., Aumailley, M., Martin, G.R. & Feldmann, R.J. (1986). Localization of binding sites for laminin, heparan sulfate proteoglycan and fibronectin on basement membrane (type IV) collagen. *J. Mol. Biol.* **189**, 205–216.

Leivo, I., Vaheri, A., Timpl, R. & Wartiovaara, J. (1980). Appearance and distribution of collagens and laminin in the early mouse embryo. *Dev. Biol.* **76**, 100–14.

Li, D., Mukai, K., Suzuki, T., Suzuki, R., Yamashita, S., Mitani, F. & Suematsu, M. (2007). Adrenocortical zonation factor 1 is a novel matricellular protein promoting integrin-mediated adhesion of adrenocortical and vascular smooth muscle cells. *FEBS J.* **274**, 2506–22.

Matsumoto, H., Ma, W., Smalley, W., Trzaskos, J., Breyer, R.M. & Dey, S.K. (2001). Diversification of cyclooxygenase-2-derived prostaglandins in ovulation and implantation. *Biol. Reprod.* **64**, 1557–65.

Matsumoto, H., Daikoku, T., Wang, H., Sato, E. & Dey, S.K. (2004). Differential expression of ezrin/radixin/moesin (ERM) and ERM-associated adhesion molecules in the blastocyst and uterus suggests their functions during implantation. *Biol. Reprod.* **70**, 729–36.

McRae, A.C. & Church, R.B. (1990). Cytoplasmic projections of trophectoderm distinguish implanting from preimplanting and implantation-delayed mouse blastocytes. *J. Reprod. Fertil.* **88**, 31–40.

Mohan, M., Hurst, A.G. & Malayer, J.R. (2004). Global gene expression analysis comparing bovine blastocysts flushed on day 7 or produced *in vitro*. *Mol. Reprod. Dev.* **68**, 288–98.

Mukai, K., Mitani, F., Nagasawa, H., Suzuki, R., Suzuki, T., Suematsu, M. & Ishimura, Y. (2003). An inverse correlation between expression of a preprocathepsin B-related protein with cysteine-rich sequences and steroid 11beta-hydroxylase in adrenocortical cells. *J. Biol. Chem.* **278**, 17084–92.

Murray, J.C., Stingl, G., Kleinman, H.K., Martin, G.R. & Katz, S.I. (1979). Epidermal cells adhere preferentially to type IV (basement membrane) collagen. *J. Cell Biol.* **80**, 197–202.

Nilsson, O. (1966). Structural differentiation of luminal membrane in rat uterus during normal and experimental

implantations. *Zeitschrift fur Anatomie und Entwicklungsgeschichte* **125**, 152–9.

Paria, B.C., Huet-Hudson, Y.M. & Dey, S.K. (1993). Blastocyst's state of activity determines the "window" of implantation in the receptive mouse uterus. *Proc. Natl. Acad. Sci. USA* **90**, 10159–62.

Paria, B.C., Ma, W., Tan, J., Raja, S., Das, S.K., Dey, S.K. & Hogan, B.L. (2001). Cellular and molecular responses of the uterus to embryo implantation can be elicited by locally applied growth factors. *Proc. Natl. Acad. Sci. USA* **98**, 1047–52.

Psychoyos, A. (1973). Endocrine control of egg implantation. In: *Handbook of Physiology* (Greep, R.O., Astwood, E.B. & Geiger, S.R., eds) American Physiological Society, Washington, DC, pp. 187–215.

Rinaudo, P. & Schultz, R.M. (2004). Effects of embryo culture on global pattern of gene expression in preimplantation mouse embryos. *Reproduction* **128**, 301–11.

Rinaudo, P.F., Giritharan, G., Talbi, S., Dobson, A.T. & Schultz, R.M. (2006). Effects of oxygen tension on gene expression in preimplantation mouse embryos. *Fertil. Steril.* **86**, 1252–65, 1265.e1–36.

Rubin, K., Hook, M., Obrink, B. & Timpl, R. (1981). Substrate adhesion of rat hepatocytes: mechanism of attachment to collagen substrates. *Cell* **24**, 463–70.

Salamat, M., Gotz, W., Werner, J. & Herken, R. (1993). Ultrastructural localization of lectin-binding sites in different basement membranes. Histochem. J. **25**, 464–8.

Schilperoort-Haun, K.R. & Menino, A.R., Jr. (2002a). Evaluation of extracellular matrix proteins and tissue inhibitor of matrix metalloproteinases-2 on bovine inner cell mass outgrowth *in vitro*. *In Vitro Cell. Dev. Biol.* **38**, 41–7.

Schilperoort-Haun, K.R. & Menino, A.R., Jr. (2002b). Factors affecting cellular outgrowth from porcine inner cell masses *in vitro*. *J. Anim. Sci.* **80**, 2671–80.

Sherman, M.I., Gay, R., Gay, S. & Miller, E.J. (1980). Association of collagen with preimplantation and peri-implantation mouse embryos. *Dev. Biol.* **74**, 470–8.

Stephens, L.E., Sutherland, A.E., Klimanskaya, I.V., Andrieux, A., Meneses, J., Pedersen, R.A. & Damsky, C.H. (1995). Deletion of beta 1 integrins in mice results in inner cell mass failure and peri-implantation lethality. *Genes Dev.* **9**, 1883–95.

Summers, M.C., McGinnis, L.K., Lawitts, J.A., Raffin, M. & Biggers, J.D. (2000). IVF of mouse ova in a simplex optimized medium supplemented with amino acids. *Hum. Reprod.* (Oxford, England), **15**, 1791–801.

Sutherland, A.E., Calarco, P.G. & Damsky, C.H. (1988). Expression and function of cell surface extracellular matrix receptors in mouse blastocyst attachment and outgrowth. *J. Cell Biol.* **106**, 1331–48.

Thorsteinsdottir, S. (1992). Basement membrane and fibronectin matrix are distinct entities in the developing mouse blastocyst. *Anat. Rec.* **232**, 141–9.

Wang, H. & Dey, S.K. (2006). Roadmap to embryo implantation: clues from mouse models. *Nat. Rev.* **7**, 185–99.

Wartiovaara, J., Leivo, I. & Vaheri, A. (1979). Expression of the cell surface-associated glycoprotein, fibronectin, in the early mouse embryo. *Dev. Biol.* **69**, 247–57.

Yelian, F.D., Yang, Y., Hirata, J.D., Schultz, J.F. & Armant, D.R. (1995). Molecular interactions between fibronectin and integrins during mouse blastocyst outgrowth. *Mol. Reprod. Dev.* **41**, 435–48.

Yohkaichiya, T., Hoshiai, H., Uehara, S. & Yajima, A. (1988). Fibronectin localization in the mouse embryo from the two cell stage to the morula stage. *Tohoku J. Exp. Med.* **154**, 95–100.

Yoshinaga, K. & Adams, C.E. (1966). Delayed implantation in the spayed, progesterone treated adult mouse. *J. Reprod. Fertil.* **12**, 593–5.

Zetter, B.R. & Martin, G.R. (1978). Expression of a high molecular weight cell surface glycoprotein (LETS protein) by preimplantation mouse embryos and teratocarcinoma stem cells. *Proc. Natl. Acad. Sci. USA* **75**, 2324–8.

Eukaryotic Cell

Outer Dynein Arm Light Chain 1 Is Essential for Controlling the Ciliary Response to Cyclic AMP in Paramecium tetraurelia

Osamu Kutomi, Manabu Hori, Masaki Ishida, Takashi Tominaga, Hiroyuki Kamachi, France Koll, Jean Cohen, Norico Yamada and Munenori Noguchi

Eukaryotic Cell **2012, 11(5):645. DOI: 10.1128/EC.05279-11. Published Ahead of Print 16 March 2012.**

EC
Journals.ASM.org

Outer Dynein Arm Light Chain 1 Is Essential for Controlling the Ciliary Response to Cyclic AMP in *Paramecium tetraurelia*

Osamu Kutomi,[a] Manabu Hori,[b,c] Masaki Ishida,[d] Takashi Tominaga,[e] Hiroyuki Kamachi,[a] France Koll,[c] Jean Cohen,[c] Norico Yamada,[f]* and Munenori Noguchi[a]

Department of Environmental Biology and Chemistry, Graduate School of Science and Engineering, University of Toyama, Toyama, Japan[a]; Division of Environmental Science and Engineering, Graduate School of Science and Engineering, Yamaguchi University, Yamaguchi, Japan[b]; Centre de Génétique Moléculaire, CNRS, Gif-sur-Yvette, France[c]; School of Science Education, Nara University of Education, Nara, Japan[d]; Department of Neurophysiology, Kagawa School of Pharmaceutical Sciences, Tokushima Bunri University, Kagawa, Japan[e]; and Department of Environmental Biology and Chemistry, Faculty of Science, University of Toyama, Toyama, Japan[f]

The individual role of the outer dynein arm light chains in the molecular mechanisms of ciliary movements in response to second messengers, such as Ca^{2+} and cyclic nucleotides, is unclear. We examined the role of the gene termed the outer dynein arm light chain 1 (LC1) gene of *Paramecium tetraurelia* (*ODAL1*), a homologue of the outer dynein arm LC1 gene of *Chlamydomonas reinhardtii*, in ciliary movements by RNA interference (RNAi) using a feeding method. The *ODAL1*-silenced (*ODAL1*-RNAi) cells swam slowly, and their swimming velocity did not increase in response to membrane-hyperpolarizing stimuli. Ciliary movements on the cortical sheets of *ODAL1*-RNAi cells revealed that the ciliary beat frequency was significantly lower than that of control cells in the presence of ≥1 mM Mg^{2+}-ATP. In addition, the ciliary orientation of *ODAL1*-RNAi cells did not change in response to cyclic AMP (cAMP). A 29-kDa protein phosphorylated in a cAMP-dependent manner in the control cells disappeared in the axoneme of *ODAL1*-RNAi cells. These results indicate that *ODAL1* is essential for controlling the ciliary response by cAMP-dependent phosphorylation.

Eukaryotic cilia and flagella are cell organelles for motility and sensing and have various important roles in biological processes. The locomotor behavior of *Paramecium* depends on ciliary movements. The ciliary movements are controlled by changes in the membrane potential that regulate the intraciliary concentrations of Ca^{2+} and cyclic nucleotides. For example, membrane depolarization in response to a mechanical or chemical stimulus applied to the anterior membrane causes an increase in the intraciliary Ca^{2+} concentration (13), which results in a change in the ciliary orientation toward the anterior direction of the cell (ciliary reversal) and a change in the swimming direction (24). Membrane hyperpolarization in response to a mechanical or chemical stimulus applied to the posterior membrane causes an increase in the intraciliary cyclic AMP (cAMP) concentration (38). This induces an increase in the ciliary beat frequency and changes the ciliary orientation to a more posterior orientation, which causes faster forward swimming (11, 25–30). In addition, cAMP suppresses Ca^{2+}-induced ciliary reversal (11, 25–30). However, the molecular bases of the control mechanism of ciliary movements are unclear.

The outer and inner dynein arms, which are multisubunit complexes attached to the outer surface of the peripheral microtubule doublets, generate forces that cause ciliary and flagellar movements. These multisubunit complexes are composed of one or more catalytic heavy chains (HCs) associated with several intermediate chains (ICs) and light chains (LCs). It has been postulated that certain outer dynein arm LCs are responsible for the regulation of ciliary and flagellar movements. For example, the outer dynein arm of *Chlamydomonas reinhardtii* comprises 3 HCs, 2 ICs, and 11 LCs (19). Among the LCs, LC1 associates directly with the catalytic motor domain of γHC (8, 33, 45). The expression of dominant negative LC1 mutant proteins in wild-type *C. reinhardtii* cells showed significant alterations in the flagellar waveform (33). A *Trypanosoma brucei* outer dynein arm LC1 knockdown mutant created by RNA interference (RNAi) exhibited slow backward propulsion and a reversed flagellar beat (6). In addition, the loss of LC1 induced the destabilization of the outer dynein arms. In the planarian *Schmidtea mediterranea*, a reduction in levels of LC1 by RNAi caused a significant drop in the ciliary beat frequency and abolished the ability of beating cilia to form metachronal waves (36). However, the precise role of LC1 of dynein complexes in the molecular mechanisms of ciliary and flagellar movements is unclear. The control of ciliary and flagellar movements depends on second messengers, such as Ca^{2+} and cyclic nucleotides. Therefore, determining how defects of LC1 affect the regulation of the ciliary and flagellar responses to second messengers is essential to an understanding of the role of the dynein subunits in the molecular mechanisms.

We have shown previously that a cortical sheet, an experimental system that we developed, is a useful tool to analyze the ciliary movements of *Paramecium* (26–29, 31). In addition, the *Paramecium tetraurelia* genome database, a ciliary proteome database, and protocols for genetic engineering by RNAi are available (1–4, 14). Therefore, ciliated *Paramecium* could be a useful model organism to study the role of axonemal proteins in the molecular mechanisms of ciliary movements.

In this study, we focused on a gene termed the outer dynein

Received 31 October 2011 Accepted 2 March 2012
Published ahead of print 16 March 2012
Address correspondence to Munenori Noguchi, noguchi@sci.u-toyama.ac.jp.
* Present address: Department of Natural History Sciences, Graduate School of Science, Hokkaido University, Sapporo, Japan.
Supplemental material for this article may be found at http://ec.asm.org/.

doi:10.1128/EC.05279-11

arm light chain 1 gene of *P. tetraurelia* (*ODAL1*), a homologue of the LC1 gene of *C. reinhardtii*. We analyzed the role of *ODAL1* in ciliary movements by RNAi using a feeding method (14). Our results indicate that the *ODAL1* gene is essential for controlling cAMP-dependent ciliary movement.

MATERIALS AND METHODS

Cell culture. *P. tetraurelia* (stock 7.2B) cells were cultured in a hay infusion bacterized with *Enterobacter aerogenes* and supplemented with 0.8 μg/ml β-sitosterol according to standard procedures (40). The cells were grown to the late logarithmic phase at 25°C.

Gene silencing by RNAi using the feeding method. The open reading frame region of *ODAL1* (GenBank accession no. XM_001446309) was amplified by PCR and cloned into the Litmus28i vector (New England BioLabs) between two T7 promoters. The amplification primers used were f1 (ATGGCAAAGACAACTTGTG) and r1 (TCATTTGACAGTGG TTGTAG). The resulting constructs were used for the transformation of HT115, an RNase III-deficient strain of *Escherichia coli* with an isopropyl-β-D-thiogalactopyranoside (IPTG)-inducible T7 polymerase (42). RNAi gene silencing was performed according to a feeding method described previously by Galvani and Sperling (14), with modifications. Wild-type paramecia were incubated in a culture medium containing 0.8 μg/ml β-sitosterol, 100 μg/ml ampicillin, and 0.4 mM IPTG. Gene silencing was initiated by the addition of double-stranded RNA-expressing bacteria to the culture medium (14). One day or two days after the induction of gene silencing, the cells were used for the experiments in this study. The phenotypes of *ODAL1*-silenced (*ODAL1*-RNAi) cells were the same after 1 day and 2 days of gene silencing. Nonsilenced *P. tetraurelia* cells were used as the control cells. As a negative control, we used *ND7* silencing, which affects trichocyst exocytosis without altering the *ODAL1* gene or any other cellular function (16, 37). Furthermore, we analyzed the off-target effect of *ODAL1* silencing using the ParameciumDB *P. tetraurelia* genome database (http://paramecium.cgm.cnrs-gif.fr/) (1).

Competitive PCR. One microgram of each poly(A)$^+$ RNA was reverse transcribed by using PrimeScript reverse transcriptase (TaKaRa Bio Inc., Japan). A 2-μl aliquot of cDNA was added to each PCR mixture, which also contained 1.5 units of *Taq* DNA polymerase, 10 mM Tris-HCl (pH 9.0 at room temperature), 50 mM KCl, 0.1% Triton X-100, 2 mM $MgCl_2$, 0.2 μM deoxynucleoside triphosphates (dNTPs), and 0.4 μM each primer described above. The amplification protocol consisted of one cycle at 94°C for 1 min, 54°C for 30 s, and 72°C for 60 s; 24 cycles at 94°C for 20 s, 55°C for 20 s, and 72°C for 30 s; and a final extension step at 72°C for 5 min. To quantitatively compare the PCR products, we determined the exponential phase of amplification by performing amplification for 15, 20, 25, and 30 cycles, using the *ODAL1* primers 5′-CTTTCTTCAAATGCAATAG-3′ (sense) and 5′-CATTTAGGGTCATCTTTC-3′ (antisense). In addition, as an internal control for cDNA quantity and quality, we amplified the gene for beta-actin by using the primers 5′-TTGATTATGAAGAGGAAA TG-3′ (sense) and 5′-TCTGTGGACAATGGTTGG-3′ (antisense). Amplified PCR products were electrophoresed in 2.0% agarose gels and visualized by ethidium bromide staining. To quantify the relative amounts of each PCR product, the ethidium-stained gels were reversed and analyzed by using ImageJ (National Institutes of Health). The ratios of *ODAL1* mRNA to beta-actin mRNA were calculated based on the densities of the PCR products (7, 15, 32, 39).

Assays of swimming behavior. Approximately 50 μl of a cell culture containing 40 to 50 live cells was placed by a micropipette onto a depression slide. Membrane-hyperpolarizing stimulation was performed by the addition of $CaCl_2$ to attain a Ca^{2+} concentration of 2 mM in the cell culture (22). After the addition of $CaCl_2$, the behaviors of individual cells were observed under a VCT-VBITVb digital microscope (Shimadzu, Japan) and recorded for 1 s. A sequential image of the swimming path was prepared from the recorded frames by using Motic Images Plus 2.1S (Shimadzu, Japan). The forward swimming velocity was determined by measuring the length of the swimming path by using ImageJ. Membrane-depolarizing stimulation was performed by the addition of KCl to attain a K^+ concentration of 50 mM in the cell culture. After the addition of KCl, backward swimming was observed by using a VCT-VBITVb digital microscope, and the duration of the backward swimming was determined.

Preparation and reactivation of cortical sheets from live cells. The preparation of cortical sheets from live cells (intact cortical sheets) was performed according to methods described in our previous paper (31), with slight modifications. Concentrated cells were washed by centrifugation with an ice-cold washing medium containing 2 mM EDTA, 50 mM potassium acetate, and 10 mM Tris-maleate buffer (pH 7.0). The loose pellet of cells was resuspended in 1 ml of an ice-cold potassium acetate solution containing 50 mM potassium acetate and 10 mM Tris-maleate buffer (pH 7.0). The cells were pipetted once or twice through a glass pipette with a small inside diameter (approximately 0.15 mm) to tear or nick the cell cortex. This cell suspension was used for the reactivation experiments. A simple perfusion chamber was prepared by placing the sample between a slide and a coverslip. The slide and coverslip were separated by a thin layer of Vaseline applied to two opposite edges of the coverslip. To observe the reactivation of cilia on the sheet of cell cortex, 50 μl of the sample was gently placed onto a glass slide, and a coverslip with Vaseline was placed over the sample. Solutions were then perfused through the narrow opening at one of the edges of the coverslip, while the excess fluid was drained from the opposite end with the aid of small pieces of filter paper. During the first perfusion using a reference potassium acetate solution, some torn cell cortex adhered flat to the glass surface.

Cortical sheets were perfused successively with reactivation solutions. All reactivation solutions contained 50 mM potassium acetate and 10 mM Tris-maleate buffer (pH 7.0) as well as a component(s), such as $MgCl_2$, ATP, and cyclic nucleotide, as noted in Results and the figure legends. The free Ca^{2+} concentration of 2×10^{-6} M and lower in the reactivation solutions was controlled by using Ca-EGTA buffer (34), using 1 mM EGTA; a concentration of $>2 \times 10^{-6}$ M was obtained by the addition of an adequate amount of $CaCl_2$ to a reactivation solution without EGTA. The reactivation of cilia was carried out at 22°C to 25°C. To determine the ciliary beat frequency, the reactivation of cilia on intact cortical sheets was performed in the presence of 5 μM cyclic GMP (cGMP) throughout, because reactivated cilia without cGMP beat in an abnormal manner to some extent (27).

The ciliary orientation was observed in the presence of 30% glycerol to clearly determine the ciliary orientation (26, 28, 29). Intact cortical sheets were demembranated by perfusion with a Triton solution containing 0.05% Triton X-100, 1 mM EGTA, 1 mM $MgCl_2$, 50 mM potassium acetate, and 10 mM Tris-maleate (pH 7.0) for 1 min and then washed by perfusion with the same solution without Triton X-100 to remove Triton X-100. The demembranated cortical sheets were incubated in a glycerol solution containing 30% glycerol, 1 mM EGTA, 1 mM $MgCl_2$, 50 mM potassium acetate, and 10 mM Tris-maleate (pH 7.0) for 5 min. The cilia were reactivated by perfusion with reactivation solutions containing 30% glycerol, 1 mM ATP, 1 mM $MgCl_2$, 50 mM potassium acetate, and 10 mM Tris-maleate (pH 7.0) as well as Ca^{2+} and cAMP, as noted in Results and the figure legends. In the presence of 30% glycerol, the reactivated cilia on the cortical sheets exhibited only a restricted beat with a small amplitude. However, the pointing directions of the cilia changed in response to Ca^{2+} and cAMP reversibly (26, 28, 29).

Observation and recording of reactivated cilia. The reactivated cilia on cortical sheets were observed under a dark-field microscope equipped with a 100-W mercury light source, a heat filter, and a green filter. The ciliary movements were recorded by using an HAS-220 high-speed camera (Ditect, Japan). To determine the ciliary beat frequency, recording was performed at 600 frames per s, and to determine the ciliary direction, recording was performed at 100 frames per s.

Analysis of ciliary movements on cortical sheets. The movements of the reactivated cilia on intact cortical sheets were analyzed by using ImageJ. We analyzed cilia on the left-hand field of the sheet, defining the surface area of the anatomical left-hand side as the left-hand field of the

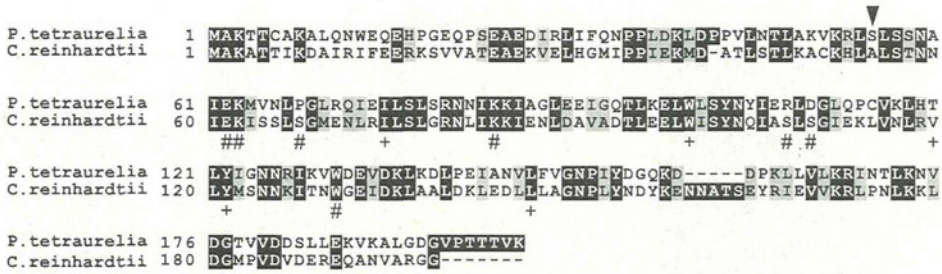

FIG 1 Sequence comparison between *P. tetraurelia* and *C. reinhardtii*. The deduced amino acid sequence alignment between *ODAL1* of *P. tetraurelia* (GenBank accession no. XM_001446309) and the *C. reinhardtii* LC1 gene (accession no. AF112476) was generated with Clustal W (http://www.ebi.ac.uk/Tools/clustalw/) and was displayed by using Boxshade (http://www.ch.embnet.org/software/BOX_form.html). Black boxes indicate identical residues. Gray boxes indicate conservative substitutions. Most of the key residues were conserved, including the γHC catalytic domain binding sites (+) and the tubulin binding sites (#). The arrowhead indicates the putative amino acid (S55), which is strongly predicted to become phosphorylated in a cAMP-dependent manner by the NetPhos 2.0 program (9).

cortical sheets (28). The beat frequency of the reactivated cilia was determined by the direct measurement of the ciliary beat cycle by monitoring the recorded video images frame by frame (31). The method for determining the ciliary orientation was essentially the same as that described in our previous papers (26, 28, 29). Three cilia on several independent cortical sheets from at least two independent RNAi preparations were measured for ciliary beat frequency and ciliary orientation.

Isolation of cilia. Collected cells were washed twice with a washing solution containing 2 mM KCl, 2 mM $CaCl_2$, and 10 mM Tris-maleate (pH 7.0). Cells were deciliated by dibucaine treatment according to methods described previously by Mogami and Takahashi (23), with slight modifications (29). Cilia were isolated from cell bodies by centrifugation twice at 600 × *g* for 5 min. The supernatant was centrifuged at 7,700 × *g* for 10 min to pellet the cilia. The pellet was resuspended in TMKE solution (10 mM Tris-maleate [pH 7.0], 5 mM $MgCl_2$, 20 mM potassium acetate, and 1 mM EGTA) containing 0.3 mM phenylmethylsulfonyl fluoride and centrifuged. The pellet was rewashed with TMKE solution. Each step of the cilium isolation was monitored by dark-field microscopy. Isolated cilia were then treated with a demembranation solution containing 0.1% Triton X-100 in TMKE solution for 10 min at 0°C. The suspension was centrifuged to pellet the axonemes. Triton X-100 was removed from the axonemes by washing twice with TMKE solution. The pellet of the axonemes was suspended in a small amount of TMKE solution.

Phosphorylation of axonemal proteins. The *in vitro* phosphorylation of the axonemes was performed according to methods described previously by Hamasaki et al. (18), with slight modifications. The reaction mixture contained 75 μg axonemes and 30% glycerol in 80 μl TMKE solution as well as test substances. Phosphorylation by endogenous protein kinases was started by the addition of 20 μl of [γ-^{32}P]ATP to attain a final concentration of 2 μM ATP. The ATP concentration of [γ-^{32}P]ATP was 10 μM, and the radioactivity was adjusted to 10 μCi with adenosine 5′-[γ-^{32}P]triphosphate (specific activity, 6,000 Ci/mmol; MP Biomedicals Inc., Solon, OH). Immediately after 10 min of incubation at 0°C, the reaction mixture was centrifuged at 10,000 × *g* for 10 min. The pellet was directly suspended in SDS sample buffer (2% SDS, 5% 2-mercaptoethanol, 10% glycerol, 0.5% bromophenol blue, and 62.5 mM Tris-HCl [pH 6.8]) and incubated at 100°C for 2 min. These SDS-treated samples were then subjected to SDS-PAGE or stored at −20°C for further use. The protein concentration was determined according to methods described previously by Lowry et al. (21), using bovine serum albumin as a standard.

SDS-PAGE and autoradiography. SDS-PAGE was performed by a modification of a procedure described previously by Laemmli (20), using 3-to-15% linear gradient acrylamide gels containing a 0 to 19% glycerol gradient run on a 20- by 16- by 0.1-cm slab gel. The gels were stained with Coomassie blue R-250 for 15 min or with silver (10) and dried on filter paper. Molecular weight standards were obtained from Bio-Rad (Hercules, CA). To produce the autoradiograms, an imaging plate (IP; Fujifilm Corp., Tokyo, Japan) was placed over the dried gels for 2 days. After exposure, the IP was scanned by using a bioimaging analyzer system (BAS-1800; Fujifilm Corp.).

Electron microscopy. For electron microscopy, cells were fixed in 1% (vol/vol) glutaraldehyde in 0.05 M cacodylate buffer (pH 7.2) for 1 h at room temperature. The cells were washed and postfixed in 1% (wt/vol) OsO_4 for 1 h at room temperature. Postfixation was followed by washing in distilled water and then dehydration in a series of increasing concentrations of ethanol and, finally, 100% propylene oxide. The cells were flat embedded in Quetol 812 (Nisshin EM Co., Ltd., Japan). Following evacuation and hardening, the cells were cut out of the block and glued onto another polymerized preshaped block. These cells were serially sectioned in a longitudinal orientation, and all of the sections were picked up on Formvar-supported grids having one large opening. The grids were placed in chronological order so that the exact position of each section within the entire series could be determined. A diamond knife (Nisshin EM Co., Ltd., Tokyo, Japan) and Ultracut E (Reichert, Buffalo, NY) were used for sectioning. Sections were then stained at room temperature with uranyl acetate (43) and lead citrate (35) for 7 min and 3 min, respectively. A transmission electron microscope (H-7000; Hitachi, Tokyo, Japan) operated at 75 kV was used throughout the study.

RESULTS

Characteristics of *ODAL1*. The *ODAL1* gene of *P. tetraurelia* (GenBank accession no. XM_001446309) encodes a protein whose predicted sequence is 38% identical to outer dynein arm LC1 of *C. reinhardtii* (accession no. AF112476), and such a protein was detected in the *P. tetraurelia* genome database and the ciliary proteome database (1–4). The *ODAL1* gene includes the conservation of most residues that directly bind the outer dynein arm γHC catalytic motor domain and tubulin (8, 33, 45) (Fig. 1). It is presumed that the *ODAL1* product has a molecular mass of 22 kDa. The cAMP-dependent phosphorylation site was predicted by using NetPhosK 2.0 (9) (Fig. 1).

Confirmation of *ODAL1* silencing by RNAi. We confirmed the effect of *ODAL1* silencing by RNAi using competitive PCR. *ODAL1* mRNA was expressed over 2-fold compared with beta-actin mRNA in nonsilenced cells (control) (Fig. 2). When the paramecia were fed *E. coli* including a knockdown plasmid, however, the amount of *ODAL1* mRNA was strikingly decreased, even within 1 day after feeding (Fig. 2). Compared to control cells, the level of *ODAL1* mRNA was 6-fold lower in *ODAL1*-silenced paramecia.

Furthermore, the off-target effect of *ODAL1* silencing was analyzed. For *ODAL1* silencing, the RNAi off-target has four genes: 3

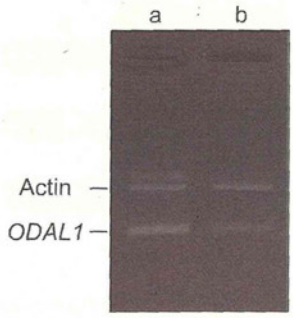

FIG 2 Competitive PCR of *ODAL1*. Shown are electrophoresis images of ethidium bromide-stained gels of *ODAL1* and beta-actin expression in control cells (lane a) and *ODAL1*-RNAi cells (1 day after the induction of gene silencing) (lane b). Each silencing paramecium was grown at 28°C and harvested at 1 day after feeding. One microgram of poly(A)$^+$ RNA of each culture was PCR amplified by using primers specific for the *ODAL1* and beta-actin genes for 25 cycles. Actin and *ODAL1* indicate the PCR products of the beta-actin (loading control) and the *ODAL1* genes, respectively.

genes are itself and its ohnologues, and the other has a completely different function, but its inactivation by this RNAi is very unlikely, since only a single 23-nucleotide (nt) siRNA can target it (data not shown). Therefore, it seems that there are no off-targets and that the RNAi insert is specific.

Phenotypes of *ODAL1*-silenced cells. We examined the phenotypes of *ODAL1*-silenced (*ODAL1*-RNAi) cells. Control cells swam at approximately 0.8 mm/s and showed a significant increase in the forward swimming velocity in response to hyperpolarizing stimulation by the addition of $CaCl_2$ to attain a Ca^{2+} concentration of 2 mM (Fig. 3A and B). In contrast, *ODAL1*-RNAi cells swam at half the swimming velocity of the control cells. Moreover, *ODAL1*-RNAi cells did not show a significant increase in the forward swimming velocity in response to hyperpolarizing stimulation (Fig. 3A and B).

Control cells exhibited backward swimming for approximately 10 s in response to depolarizing stimulation by the addition of KCl to attain a K^+ concentration of 50 mM. In contrast, *ODAL1*-RNAi cells exhibited a long period of backward swimming after the depolarizing stimulation (Fig. 3C). They also exhibited a short period of backward swimming (within 1 s), an "avoiding reaction," frequently seen in culture medium without the depolarizing stimulant (see Movie S1 in the supplemental material). The phenotypes of *ND7*-silenced (*ND7*-RNAi) cells were the same as those of the control cells (data not shown).

Effects of *ODAL1* silencing on ciliary beat frequency in response to Mg^{2+}-ATP. The effects of *ODAL1* silencing on the ciliary beat frequency were determined at various concentrations of Mg^{2+}-ATP by using intact cortical sheets. The ciliary beat frequency of the control cells increased with increasing Mg^{2+}-ATP concentrations up to 8 mM (Fig. 4, and see Movie S2A in the supplemental material). The apparent K_m and V_{max} were 0.80 mM and 52 Hz, respectively. In contrast, the ciliary beat frequency of *ODAL1*-RNAi cells did not increase in the presence of $\geq$1 mM Mg^{2+}-ATP (Fig. 4, and see Movie S2B in the supplemental material). The apparent K_m and V_{max} of *ODAL1*-RNAi cells (2 days after the induction of gene silencing) were 0.22 mM and 21 Hz, respectively. However, the reactivated cilia of *ODAL1*-RNAi cells showed a normal beat cycle that consisted of an effective stroke and a recovery stroke (37) (see Movie S2B in the supplemental material). The ciliary beat frequency of *ND7*-RNAi cells was essentially the same as that of the control (Fig. 4).

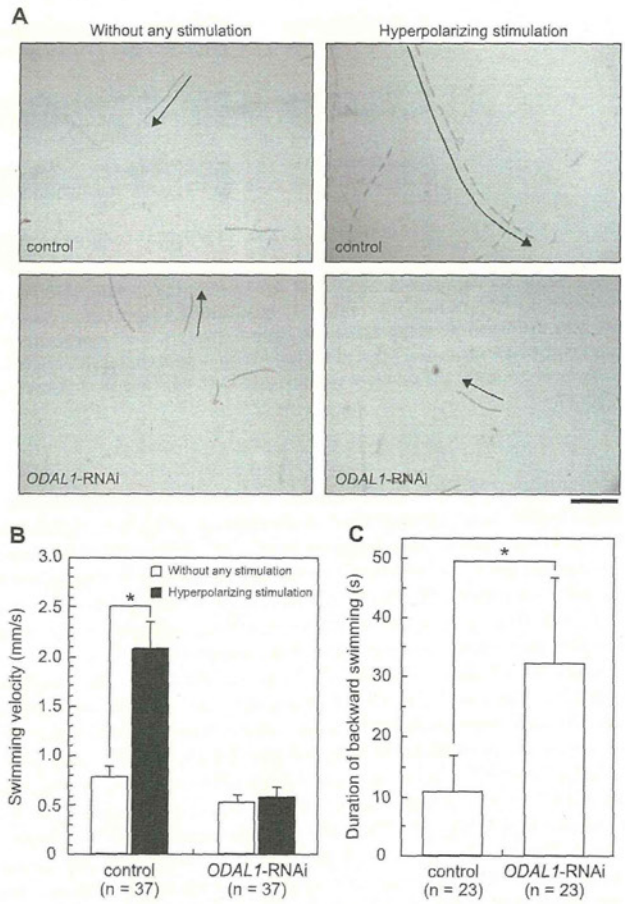

FIG 3 Phenotypes of *ODAL1*-RNAi cells. Swimming behaviors of control cells and *ODAL1*-RNAi cells (2 days after the induction of gene silencing) were observed under certain conditions. Observation and recording were performed as indicated in Materials and Methods. (A) Swimming paths of live paramecia for 1 s without any stimulation and in response to hyperpolarizing stimulation by the addition of $CaCl_2$ to attain a Ca^{2+} concentration of 2 mM. The frame capture rate was 15 frames per s. The arrows indicate the swimming directions. Bar, 0.5 mm. (B) Forward swimming velocity in control cells and *ODAL1*-RNAi cells. In the case of the control, the difference between the swimming velocities under standard conditions and under conditions of hyperpolarizing stimulation was significant (*, $P < 0.01$ by t test). In the case of *ODAL1*-RNAi cells, the difference was not significant. (C) Duration of backward swimming in control and *ODAL1*-RNAi cells. Backward swimming was induced by depolarizing stimulation by the addition of KCl to attain a K^+ concentration of 50 mM. The difference between the durations of backward swimming in control and *ODAL1*-RNAi cells was significant (*, $P < 0.001$ by t test). Boxes and bars indicate means $\pm$ standard deviations (SD), respectively. The number of measurements is indicated in each panel (B and C).

Effects of *ODAL1* silencing on ciliary orientation in response to Ca^{2+} and cAMP. The effects of *ODAL1* silencing on the ciliary orientation in response to Ca^{2+} without cAMP were determined by using cortical sheets. The orientation of the reactivated cilia of the control was toward the 6-o'clock position (posterior direction of the cell) at $\leq$0.2 μM Ca^{2+} (Fig. 5A). When the cortical sheets were perfused with a reactivation solution containing $\geq$1 μM Ca^{2+}, the orientation of the cilia was toward the 12-o'clock position (anterior direction of the cell) (26, 28, 29). The changes in the

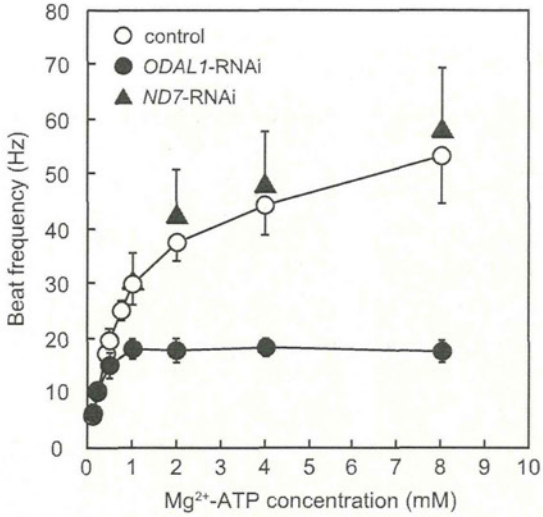

FIG 4 Effect of *ODAL1* silencing on ciliary beat frequency in response to Mg^{2+}-ATP. Changes in the ciliary beat frequency in response to an increasing Mg^{2+}-ATP concentration were determined. Intact cortical sheets from control cells, *ODAL1*-RNAi cells (2 days after the induction of gene silencing), and *ND7*-RNAi cells (2 days after the induction of gene silencing) were perfused successively with reactivation solutions containing 5 μM cGMP, 1 mM EGTA, 50 mM potassium acetate, 10 mM Tris-maleate buffer (pH 7.0), and various concentrations of Mg^{2+}-ATP. The $MgCl_2$ concentration was kept at 1 mM at an ATP concentration of ≤1 mM. The $MgCl_2$ concentration was equal to the ATP concentration at an ATP concentration of >1 mM. Values represent means ± SD (n = 5 to 13).

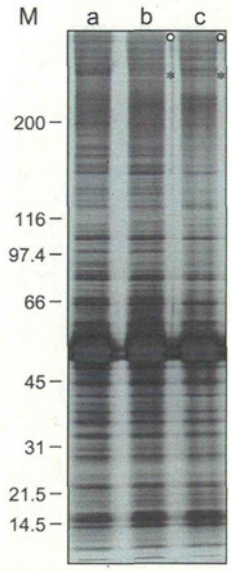

FIG 6 SDS-PAGE patterns of axonemal proteins from *ODAL1*-RNAi cells. The compositions of axonemal proteins from control (lane a), *ODAL1*-RNAi (1 day after the induction of gene silencing) (lane b), and *ODAL1*-RNAi (2 days after the induction of gene silencing) (lane c) cells were analyzed by SDS-PAGE as described in Materials and Methods. Open circles, outer dynein arm HCs; asterisks, an unidentified HC; M, M_r of markers (×10^3).

ciliary orientation of *ODAL1*-RNAi cells on cortical sheets in response to Ca^{2+} were very similar to those of the control cells (Fig. 5A).

The effects of *ODAL1* silencing on the ciliary orientation on cortical sheets in response to cAMP were determined in the presence of 2 μM Ca^{2+}. In the case of the control cells, the ciliary orientation began to change from an anterior to a posterior direction of the cell in the presence of 1 μM cAMP. At ≥10 μM cAMP, the orientation of the reactivated cilia was toward the 5-o'clock position (posterior direction of the cell). On the contrary, the ciliary orientation of *ODAL1*-RNAi cells did not change from the anterior to the posterior direction of the cell, even in the presence of 100 μM cAMP (Fig. 5B). The ciliary orientation of *ND7*-RNAi cells in response to Ca^{2+} and cAMP was essentially the same as that of control cells (Fig. 5A and B).

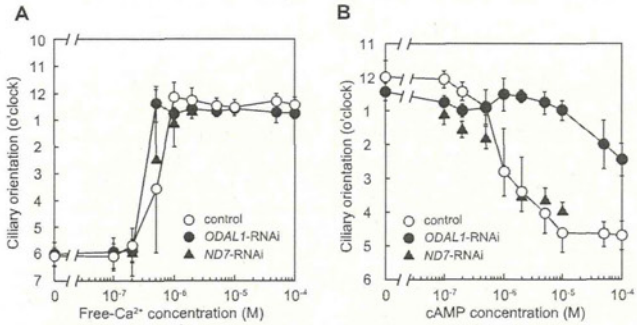

FIG 5 Effects of *ODAL1* silencing on ciliary orientation in response to Ca^{2+} and cAMP. The ciliary orientation in response to Ca^{2+} and cAMP was determined in the presence of 30% glycerol. The demembranated cortical sheets from control, *ODAL1*-RNAi (2 days after the induction of gene silencing), and *ND7*-RNAi (2 days after the induction of gene silencing) cells were perfused successively with reactivation solutions containing 30% glycerol, 1 mM ATP, 1 mM $MgCl_2$, 50 mM potassium acetate, and 10 mM Tris-maleate buffer (pH 7.0) and various concentrations of free Ca^{2+} and cAMP, as noted in the abscissas. The free Ca^{2+} concentration in the reactivation solutions was controlled as indicated in Materials and Methods. The orientation between 11 o'clock and 2 o'clock indicates a Ca^{2+}-induced ciliary reversal. (A) Changes in ciliary orientation in response to Ca^{2+} without cAMP. (B) Changes in ciliary orientation in response to cAMP in the presence of 2 μM Ca^{2+}. Values represent means ± SD (n = 5 to 6).

Change in composition of axonemal proteins after *ODAL1* silencing. The axonemal proteins of *ODAL1*-RNAi cells were analyzed by SDS-PAGE using 3-to-15% polyacrylamide gradient gels. The two HC bands were decreased to some extent in the 1-day- and 2-day-silenced *ODAL1*-RNAi cells (Fig. 6, lanes b and c). The composition of axonemal proteins was not affected by *ND7* silencing (data not shown).

Effects of *ODAL1* silencing on cAMP-dependent phosphorylation of axonemal proteins. We examined the effects of *ODAL1* silencing on the cAMP-dependent phosphorylation of axonemal proteins. In control and the *ND7*-RNAi cells, the 29-kDa and 65-kDa axonemal polypeptides were phosphorylated with 10 μM cAMP (5, 17, 26, 27, 29, 30) (Fig. 7).

In *ODAL1*-RNAi cells, the 65-kDa polypeptide was phosphorylated with 10 μM cAMP, but the phosphorylation of the 29-kDa polypeptide was not detected after 1 day of silencing (Fig. 7A). After 2 days of silencing, no phosphorylation was detected for the 29-kDa or 65-kDa polypeptide (Fig. 7B).

Effects of *ODAL1* silencing on the presence of outer and inner dynein arms within axonemes. Cross sections of cilia from the control, *ODAL1*-RNAi, and *ND7*-RNAi cells were observed by using a transmission electron microscope. In the *ODAL1*-RNAi

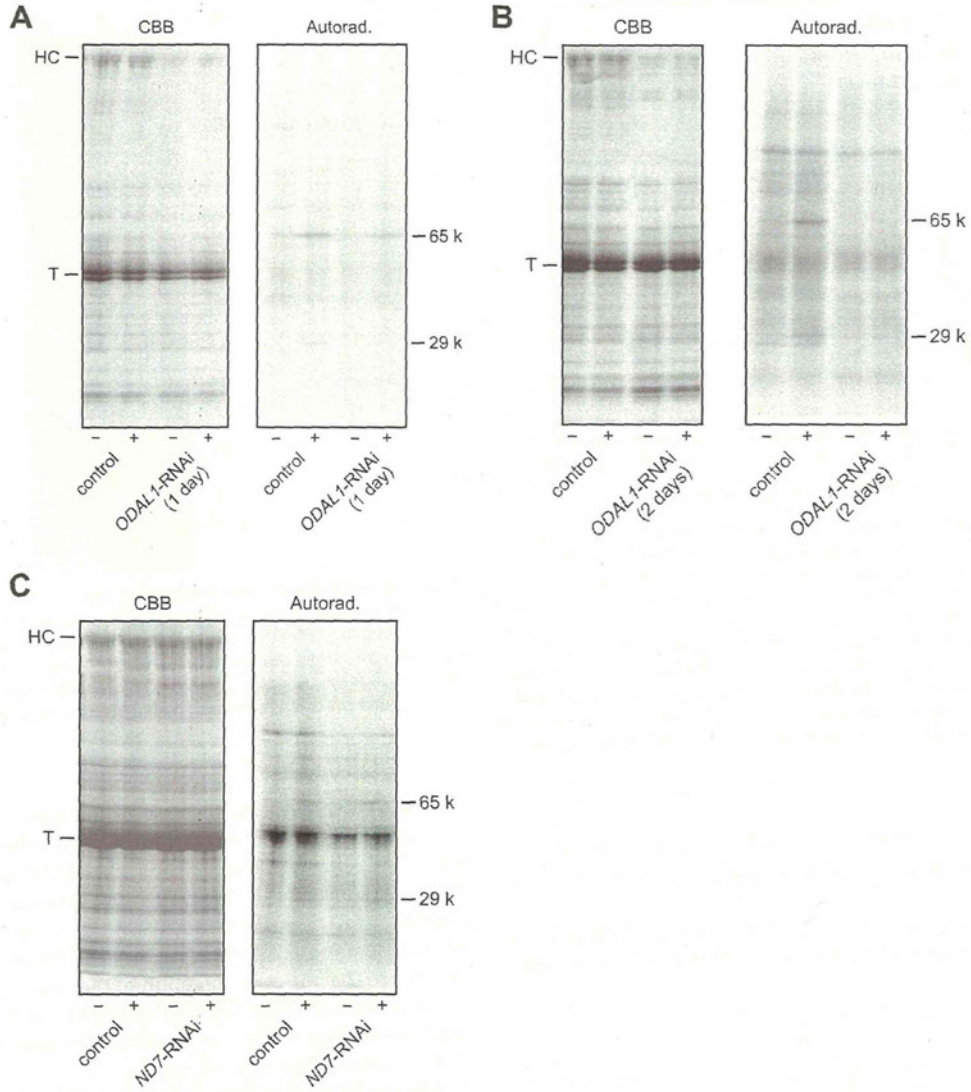

FIG 7 cAMP-dependent phosphorylation of the axonemal proteins from *ODAL1*-RNAi cells. Axonemes were labeled *in vitro* with adenosine 5′-[γ-^{32}P]triphosphate. The phosphorylated proteins were run on 3-to-15% linear gradient acrylamide gels. CBB, band pattern stained with Coomassie blue R 250; Autorad., autoradiogram. (A) Effect of *ODAL1* silencing (1 day after the induction of gene silencing) on the cAMP-dependent phosphorylation of axonemal proteins. (B) Effects of *ODAL1* silencing (2 days after the induction of gene silencing) on the cAMP-dependent phosphorylation of axonemal proteins. (C) Effects of *ND7* silencing on the cAMP-dependent phosphorylation of axonemal proteins. 65 k and 29 k indicate the cAMP-dependent phosphorylated 65-kDa and 29-kDa polypeptides in the autoradiogram, respectively. + and − indicate the presence and absence of 10 μM cAMP, respectively. HC, outer dynein arm HCs; T, tubulins.

axonemes, a couple of the outer dynein arms had disappeared randomly (indicated by arrowheads in Fig. 8A and B). The mean number of missing outer dynein arms was 3.22 ± 1.64 (n = 36) (Fig. 8D). However, the inner dynein arms of *ODAL1*-RNAi were not affected. In the *ND7*-RNAi cells, both the outer and inner dynein arms were not affected (Fig. 8C).

DISCUSSION

Outer dynein arm LC1 has been thought to be responsible for regulating ciliary and flagellar movements. For example, *C. reinhardtii* LC1 binds the outer arm dynein γHC motor domain and a doublet microtubule within the axonemal superstructure and may regulate outer dynein arm activity through a conformational switch for flagellar motility (8, 33, 45). In *T. brucei*, LC1 is necessary for proper forward flagellar motility and for a stable outer dynein arm assembly (6). LC1 of the planarian *S. mediterranea* acts in a mechanosensory feedback mechanism controlling outer arm activity (36). However, the role of outer dynein arm LC1 in the molecular mechanisms of ciliary and flagellar movements is unclear. In this study, we cloned *ODAL1* from *P. tetraurelia* using the *Paramecium* genome database and the ciliary proteome database (1–4). To clarify the role of *ODAL1* in the ciliary movements of *P. tetraurelia*, we created *ODAL1*-silenced cells by RNAi using the feeding method (14) and examined the effects of *ODAL1* silencing on the ciliary movements and the compositions of axonemal proteins. We confirmed that the *ODAL1* gene was properly silenced (Fig. 2) and that *ODAL1* silencing could have no off-target effects. Furthermore, as a negative control, we examined the

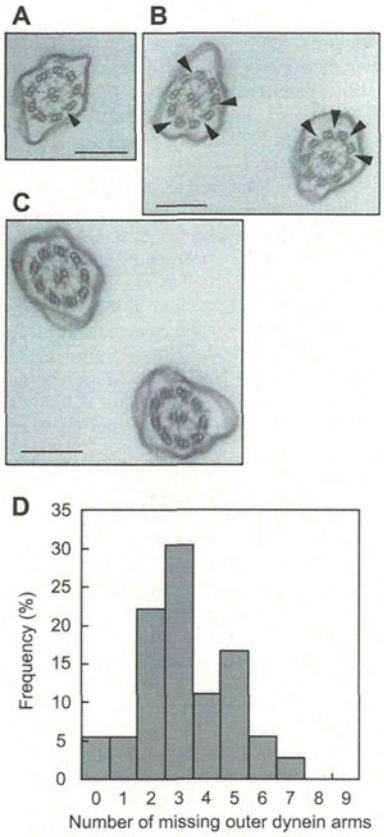

FIG 8 Transmission electron micrographs of cross sections of *ODAL1*-RNAi cilia. Typical cross-sectional images of cilia from *ODAL1*-RNAi (2 days after the induction of gene silencing) (A and B) and *ND7*-RNAi (C) cells were observed by using a transmission electron microscope. The arrowheads indicate the positions of the missing outer dynein arms on the outer doublet microtubules. Bars, 200 nm. (D) Histogram of missing outer dynein arms in *ODAL1*-RNAi axonemes. The abscissa indicates how many outer dynein arms were missing ($n = 36$).

effects of *ND7* silencing, which affects trichocyst exocytosis without altering the *ODAL1* gene or any other cellular function (16, 37). We confirmed that *ND7* silencing did not affect the ciliary movements and the compositions of axonemal proteins (Fig. 4, 5, 7C, and 8C).

We initially examined the phenotypes of *ODAL1*-RNAi cells. They swam more slowly than the control cells, and their swimming velocity did not increase in response to hyperpolarizing stimulation (Fig. 3A and B). In addition, the silenced cells showed a long period of backward swimming in response to depolarizing stimulation and, frequently, a spontaneous avoiding reaction in the absence of depolarizing stimulation (Fig. 3C, and see Movie S1 in the supplemental material). These observations suggest that *ODAL1* silencing resulted in two types of defects in the ciliary activities. The first defect is the impairment of the ability to increase the ciliary beat frequency. The second defect is apparent hypersensitivity to Ca^{2+}.

The ciliary beat frequency depends on the Mg^{2+}-ATP concentration (31) (Fig. 4, and see Movie S2A in the supplemental material). We found that the ciliary beat frequency on intact cortical sheets of *ODAL1*-RNAi cells did not increase with high concentrations of Mg^{2+}-ATP ($\geq$1 mM) (Fig. 4, and see Movie S2B in the supplemental material). This indicates that *ODAL1* silencing impairs the ability to increase the ciliary beat frequency. Therefore, the slow swimming of *ODAL1*-RNAi cells (Fig. 3A and B) is a consequence of the impairment of the ability to increase the ciliary beat frequency. The reactivated cilia of *ODAL1*-RNAi cells showed a normal beat cycle that consisted of an effective stroke and a recovery stroke (41) (see Movie S2B in the supplemental material). This suggests that *ODAL1* silencing does not impair the ciliary waveform. In *C. reinhardtii* and *Tetrahymena thermophila*, an inner dynein arm has been thought to be responsible for the regulation of the ciliary and flagellar waveforms (12, 44). Therefore, the normal ciliary waveform in *ODAL1*-RNAi cells indicates that *ODAL1* silencing does not affect the inner dynein arms of *Paramecium* (Fig. 8).

Previous analyses of ciliary movements using permeabilized cell models (Triton models) and cortical sheets have shown that $\geq$1 μM Ca^{2+} induces a ciliary reversal and backward swimming (11, 24–30). We expected that if *ODAL1*-RNAi cells showed hypersensitivity to Ca^{2+}, the ciliary orientation on cortical sheets would show a ciliary reversal in the presence of lower Ca^{2+} concentrations compared with that of the control cells. However, the threshold Ca^{2+} concentration for the ciliary orientation reversal of the control cells was almost similar to that of *ODAL1*-RNAi cells (Fig. 5A). This indicates that *ODAL1* silencing does not affect sensitivity to Ca^{2+} in the ciliary motor mechanism.

cAMP makes the ciliary orientation more posterior (26, 27, 29). Furthermore, it was shown previously that cAMP and Ca^{2+} act antagonistically in setting the ciliary orientation and that cAMP suppresses Ca^{2+}-induced ciliary reversal (11, 25–30). We analyzed the effect of *ODAL1* silencing on cAMP-dependent ciliary responses using cortical sheets. As shown in Fig. 5B, the ciliary reversal induced by 2 μM Ca^{2+} was not suppressed by cAMP in cortical sheets of *ODAL1*-RNAi cells. This result indicates that *ODAL1* silencing impairs the ciliary response to cAMP. Therefore, the phenotypes of *ODAL1*-RNAi cells, such as the longer period of backward swimming (Fig. 3C) and the spontaneous avoiding reaction in the absence of any stimulation (see Movie S1 in the supplemental material), are probably due to the apparent hypersensitivity to Ca^{2+} that is a consequence of the defect in the ciliary response to cAMP.

To test whether *ODAL1* silencing affects axonemal proteins other than the *ODAL1* product, we analyzed the composition of axonemal proteins in *ODAL1*-RNAi cells using SDS-PAGE. In the axonemes of *ODAL1*-RNAi cells, two HC bands (>200 kDa) were decreased to some extent (Fig. 6, lane b). The upper band corresponds to the outer dynein arm HC (indicated by open circles in Fig. 6). In addition, after 2 days of silencing, several bands of the axonemal proteins also decreased (Fig. 6, lane c). We observed the cross-sectional images of the *ODAL1*-RNAi axonemes with missing outer dynein arms at the level where inner dynein arms were present (Fig. 8). While such defects were rare, we did not see such axoneme cross sections in nonsilenced cells and in *ND7*-RNAi cells. Our observations indicate that as previously shown for *T. brucei* (6), in *P. tetraurelia*, the loss of *ODAL1* also destabilizes the outer dynein arms.

In *Paramecium*, a 29-kDa polypeptide (p29), an LC of the outer dynein arm (22S dynein), is phosphorylated in a cAMP-dependent manner (5, 17, 26, 27, 29, 30) (Fig. 7A and B). The sliding velocity between the outer dynein arm containing p29 and the outer doublet microtubules increased in a cAMP-dependent

manner (5, 17). Therefore, p29 is thought to play a key role in ciliary movements in response to cAMP. The deduced amino acid sequence of *ODAL1* includes several phosphorylation sites (Fig. 1), and the ciliary orientation on cortical sheets from *ODAL1*-RNAi cells lost cAMP-dependent control (Fig. 5B). This may be due to the absence of the cAMP-dependent phosphorylation of some axonemal proteins induced by *ODAL1* silencing. To test this possibility, we examined the effects of *ODAL1* silencing on the cAMP-dependent phosphorylation of axonemal proteins. As a result, the cAMP-dependent phosphorylation of p29 was not detected in the axonemes from *ODAL1*-RNAi cells (Fig. 7A and B). This result indicates that *ODAL1* silencing impairs the cAMP-dependent phosphorylation of p29. The SDS-PAGE band pattern and the observation of cross-sectional images of the *ODAL1*-RNAi axonemes showed that the outer dynein arms were decreased to some extent (Fig. 6 and 8). These results suggest that the defect in the ciliary response to cAMP caused by *ODAL1* silencing may be due to a reduction in the levels of p29 in the outer dynein arm. Our results also suggest that the structural integrity of the outer dynein arm may be essential to produce a high ciliary beat frequency. Further studies, e.g., determining ciliary movements using gene silencing for the other outer dynein arm components, will be required to clarify the mechanisms regulating the ciliary beat frequency.

In conclusion, we demonstrated that the *ODAL1* gene is essential for controlling the ciliary response by cAMP-dependent phosphorylation. The *ODAL1* product may be the p29-phosphorylatable LC of the *Paramecium* 22S dynein. The use of gene silencing by RNAi using the feeding method and the analysis of ciliary movements using cortical sheets could provide further information for an understanding of the molecular mechanism of ciliary movements.

ACKNOWLEDGMENT

This work was supported by a grant-in-aid for scientific research (C) from MEXT of Japan (grant no. 21590358 to M.H.).

REFERENCES

1. **Arnaiz O, Sperling L.** 2011. ParameciumDB in 2011: new tools and new data for functional and comparative genomics of the model ciliate *Paramecium tetraurelia*. Nucleic Acids Res. **39**:D632–D636.
2. **Arnaiz O, Cain S, Cohen J, Sperling L.** 2007. ParameciumDB: a community resource that integrates the *Paramecium tetraurelia* genome sequence with genetic data. Nucleic Acids Res. **35**:D439–D444.
3. **Arnaiz O, et al.** 2009. Cildb: a knowledgebase for centrosomes and cilia. Database **2009**:bap022. doi:10.1093/database/bap022.
4. **Aury JM, et al.** 2006. Global trends of whole-genome duplications revealed by the ciliate *Paramecium tetraurelia*. Nature **444**:171–178.
5. **Barkalow K, Hamasaki T, Satir P.** 1994. Regulation of 22S dynein by a 29-kD light chain. J. Cell Biol. **126**:727–735.
6. **Baron DM, Kabututu ZP, Hill KL.** 2007. Stuck in reverse: loss of LC1 in *Trypanosoma brucei* disrupts outer dynein arms and leads to reverse flagellar beat and backward movement. J. Cell Sci. **120**:1513–1520.
7. **Becker-André M, Hahlbrock K.** 1989. Absolute mRNA quantification using the polymerase chain reaction (PCR). A novel approach by a PCR aided transcript titration assay (PATTY). Nucleic Acids Res. **17**:9437–9446.
8. **Benashski SE, Patel-King RS, King SM.** 1999. Light chain 1 from the *Chlamydomonas* outer dynein arm is a leucine-rich repeat protein associated with the motor domain of the γ heavy chain. Biochemistry **38**:7253–7264.
9. **Blom N, Gammeltoft S, Brunak S.** 1999. Sequence- and structure-based prediction of eukaryotic protein phosphorylation sites. J. Mol. Biol. **294**:1351–1362.
10. **Blum H, Beier H, Gross HJ.** 1987. Improved silver staining of plant proteins, RNA and DNA in polyacrylamide gels. Electrophoresis **8**:93–99.
11. **Bonini NM, Nelson DL.** 1988. Differential regulation of *Paramecium* ciliary motility by cAMP and cGMP. J. Cell Biol. **106**:1615–1623.
12. **Brokaw CJ, Kamiya R.** 1987. Bending patterns of *Chlamydomonas* flagella. IV. Mutants with defects in inner and outer dynein arms indicate differences in dynein arm function. Cell Motil. Cytoskeleton **8**:68–75.
13. **Eckert R.** 1972. Bioelectric control of ciliary activity. Science **176**:473–481.
14. **Galvani A, Sperling L.** 2002. RNA interference by feeding in *Paramecium*. Trends Genet. **18**:11–12.
15. **Gilliland G, Perrin S, Blanchard K, Bunn HF.** 1990. Analysis of cytokine mRNA and DNA, detection and quantitation by competitive polymerase chain reaction. Proc. Natl. Acad. Sci. U. S. A. **87**:2725–2729.
16. **Gogendeau D, et al.** 2008. Functional diversification of centrins and cell morphological complexity. J. Cell Sci. **121**:65–74.
17. **Hamasaki T, Barkalow K, Richmond J, Satir P.** 1991. cAMP stimulated phosphorylation of an axonemal polypeptide that copurifies with the 22S dynein arm regulates microtubule translocation velocity and swimming speed in *Paramecium*. Proc. Natl. Acad. Sci. U. S. A. **88**:7918–7922.
18. **Hamasaki T, Murtaugh TJ, Satir BH, Satir P.** 1989. In vitro phosphorylation of *Paramecium* axonemes and permeabilized cells. Cell Motil. Cytoskeleton **12**:1–11.
19. **King SM, Kamiya R.** 2008. Axonemal dyneins: assembly, structure and force generation, p 131–208. *In* Witman GB (ed), The *Chlamydomonas* sourcebook: cell motility and behavior, vol 3. Academic Press, San Diego, CA.
20. **Laemmli UK.** 1970. Cleavage of structural proteins during the assembly of the head of bacteriophage T4. Nature **227**:680–685.
21. **Lowry OH, Rowebrough NJ, Farr AL, Randall RJ.** 1951. Protein measurement with the Folin phenol reagent. J. Biol. Chem. **193**:265–275.
22. **Machemer H.** 1988. Electrophysiology, p 185–215. *In* Görtz HD (ed), *Paramecium*. Springer-Verlag, Berlin, Germany.
23. **Mogami Y, Takahashi K.** 1983. Calcium and microtubule sliding in ciliary axonemes isolated from *Paramecium caudatum*. J. Cell Sci. **61**:107–121.
24. **Naitoh Y, Kaneko H.** 1972. Reactivated Triton-extracted models of *Paramecium*: modification of ciliary movement by calcium ions. Science **176**:523–524.
25. **Nakaoka Y, Ooi H.** 1985. Regulation of ciliary reversal in Triton-extracted *Paramecium* by calcium and cyclic adenosine monophosphate. J. Cell Sci. **77**:185–195.
26. **Noguchi M, Kitani T, Ogawa T, Inoue H, Kamachi H.** 2005. Augmented ciliary reorientation response and cAMP-dependent protein phosphorylation induced by glycerol in Triton-extracted *Paramecium*. Zool. Sci. **22**:41–48.
27. **Noguchi M, Kurahashi S, Kamachi H, Inoue H.** 2004. Control of the ciliary beat by cyclic nucleotides in the intact cortical sheets from *Paramecium*. Zool. Sci. **21**:1167–1175.
28. **Noguchi M, Nakamura Y, Okamoto K-I.** 1991. Control of ciliary orientation in ciliated sheets from *Paramecium*—differential distribution of sensitivity to cyclic nucleotides. Cell Motil. Cytoskeleton **20**:38–46.
29. **Noguchi M, Ogawa T, Taneyama T.** 2000. Control of ciliary orientation through cAMP-dependent phosphorylation of axonemal proteins in *Paramecium caudatum*. Cell Motil. Cytoskeleton **45**:263–271.
30. **Noguchi M, Sasaki J, Kamachi H, Inoue H.** 2003. Protein phosphatase 2C is involved in the cAMP-dependent ciliary control in *Paramecium caudatum*. Cell Motil. Cytoskeleton **54**:95–104.
31. **Noguchi M, Sawada T, Akazawa T.** 2001. ATP-regenerating system in the cilia of *Paramecium caudatum*. J. Exp. Biol. **204**:1063–1071.
32. **Noonan KE, et al.** 1990. Quantitative analysis of MDR1 (multidrug resistance) gene expression in human tumors by polymerase chain reaction. Proc. Natl. Acad. Sci. U. S. A. **87**:7160–7164.
33. **Patel-King RS, King SM.** 2009. An outer arm dynein light chain acts in a conformational switch for flagellar motility. J. Cell Biol. **186**:283–295.
34. **Portzehl H, Caldwell PC, Rüegg JC.** 1964. The dependence of contraction and relaxation of muscle fibers from the crab *Maia squinado* on the internal concentration of free calcium ions. Biochim. Biophys. Acta **79**:581–591.
35. **Reynolds ES.** 1963. The use of lead citrate at high pH as an electron-opaque stain in electron microscopy. J. Cell Biol. **17**:208–212.
36. **Rompolas P, Patel-King RS, King SM.** 2010. An outer arm dynein conformational switch is required for metachronal synchrony of motile cilia in planaria. Mol. Biol. Cell **21**:3669–3679.
37. **Ruiz F, Vayssié L, Klotz C, Sperling L, Madeddu L.** 1998. Homology-dependent gene silencing in *Paramecium*. Mol. Biol. Cell **9**:931–943.
38. **Schultz JE, Klumpp S, Benz R, Schürhoff-Goeters WJ, Schmid A.** 1992.

Regulation of adenylyl cyclase from *Paramecium* by an intrinsic potassium conductance. Science **255**:600–603.
39. **Siebert PD, Larrick JW.** 1992. Competitive PCR. Nature **359**:557–558.
40. **Sonneborn TM.** 1970. Methods in *Paramecium* research, p 241–339. *In* Prescott D (ed), Methods in cell physiology, vol 4. Academic Press, New York, NY.
41. **Sugino K, Naitoh Y.** 1982. Simulated cross-bridge patterns corresponding to ciliary beating in *Paramecium*. Nature **295**:609–611.
42. **Timmons L, Court DL, Fire A.** 2001. Ingestion of bacterially expressed dsRNAs can produce specific and potent genetic interference in *Caenorhabditis elegans*. Gene **263**:103–112.
43. **Watson ML.** 1958. Staining of tissue sections for electron microscopy with heavy metals. J. Biophys. Biochem. Cytol. **4**:475–478.
44. **Wood CR, Hard R, Hennessey TM.** 2007. Targeted gene disruption of dynein heavy chain 7 of *Tetrahymena thermophila* results in altered ciliary waveform and reduced swim speed. J. Cell Sci. **120**:3075–3085.
45. **Wu H, et al.** 2000. Solution structure of a dynein motor domain associated light chain. Nat. Struct. Biol. **7**:575–579.

nature COMMUNICATIONS

OPEN

ARTICLE

Received 8 Feb 2012 | Accepted 22 Jun 2012 | Published 24 Jul 2012

DOI: 10.1038/ncomms1971

Unfolded protein response, activated by OASIS family transcription factors, promotes astrocyte differentiation

Atsushi Saito[1], Soshi Kanemoto[1], Noritaka Kawasaki[1], Rie Asada[1], Hideo Iwamoto[1], Mami Oki[1], Hidetaka Miyagi[1], Soutarou Izumi[1], Tsukasa Sanosaka[2], Kinichi Nakashima[2] & Kazunori Imaizumi[1]

OASIS is a member of the CREB/ATF family of transcription factors and modulates cell- or tissue-specific unfolded protein response signalling. Here we show that this modulation has a critical role in the differentiation of neural precursor cells into astrocytes. Cerebral cortices of mice specifically deficient in OASIS (*Oasis*$^{-/-}$) contain fewer astrocytes and more neural precursor cells than those of wild-type mice during embryonic development. Furthermore, astrocyte differentiation is delayed in primary cultured *Oasis*$^{-/-}$ neural precursor cells. The transcription factor Gcm1, which is necessary for astrocyte differentiation in *Drosophila*, is revealed to be a target of OASIS. Introduction of Gcm1 into *Oasis*$^{-/-}$ neural precursor cells improves the delayed differentiation of neural precursor cells into astrocytes by accelerating demethylation of the *Gfap* promoter. Gcm1 expression is temporally controlled by the unfolded protein response through interactions between OASIS family members during astrocyte differentiation. Taken together, our findings demonstrate a novel mechanism by which OASIS and its associated family members are modulated by the unfolded protein response to finely control astrocyte differentiation.

[1] Department of Biochemistry, Institute of Biomedical & Health Sciences, University of Hiroshima, 1-2-3 Kasumi, Minami-ku, Hiroshima 734-8553, Japan. [2] Laboratory of Molecular Neuroscience, Graduate School of Biological Sciences, Nara Institute of Science and Technology, 8916-5 Takayama, Ikoma, Nara 630-0101, Japan. Correspondence and requests for materials should be addressed to K.I. (email: imaizumi@hiroshima-u.ac.jp).